Uncoupling interferon signaling and antigen presentation to overcome immunotherapy resistance due to JAK1 loss in melanoma

One Sentence Summary: Interferon-independent MHC class I induction restores T cell immunity.

Authors: Anusha Kalbasi*[1,3,6], Mito Tariveranmoshabad[1†], Kevin Hakimi[1†], Sarah Kremer[1], Katie M. Campbell[2], Juan M. Funes[3], Agustin Vega-Crespo[2], Giulia Parisi[2], Ameya Champekar[2], Christine Nguyen[1], Davis Torrejon[2], Daniel Shin[2], Jesse M. Zaretsky[2], Robert D. Damoiseaux[4,5,6], Daniel E. Speiser[7], Pedro P. Lopez-Casas[8], Marisol Quintero[8], Antoni Ribas[2,3,4,6,9]

Affiliations: [1]Department of Radiation Oncology, [2]Department of Medicine, Division of Hematology-Oncology, [3]Department Surgery, Division of Surgical Oncology, [4]Department of Molecular and Medical Pharmacology, [5]California NanoSystems Institute, [6]Jonsson Comprehensive Cancer Center, University of California Los Angeles (UCLA), Los Angeles, CA 90095, USA, [7]Department of Oncology, University of Lausanne, 1015 Lausanne, Switzerland. [8]Highlight Therapeutics, Madrid, Spain and [9]Parker Institute for Cancer Immunotherapy, San Francisco, CA 94129, USA. [†]These authors contributed equally.d

*To whom correspondence should be addressed: Anusha Kalbasi, M. D., Department of Radiation Oncology, Jonsson Comprehensive Cancer Center (JCCC), UCLA; B-262 Factor Building, 700 Tiverton Avenue, Los Angeles, CA 90095. Phone: (310) 267-4831; Email: anushakalbasi@mednet.ucla.edu.

Abstract:

Defects in tumor-intrinsic interferon (IFN) signaling result in failure of immune checkpoint blockade (ICB), but these cancers may still maintain sensitivity to T cell-based adoptive cell therapy (ACT). We generated models of IFN signaling defects (*Jak1*^{KO} *and Jak2*^{KO}*)* in B16 murine melanoma previously observed in patients with acquired resistance to ICB. Tumors lacking *Jak1* or *Jak2* did not respond to ICB, while ACT was effective against Jak2^{KO} tumors, but not *Jak1*^{KO} tumors where both type I and II tumor IFN signaling were defective. This is a direct result of low baseline class I major histocompatibility complex (MHC I) expression of B16 and the dependency of MHC I expression on either type I or II IFN signaling. We used genetic and pharmacologic approaches to uncouple this dependency and restore MHC I expression. Through independent mechanisms, overexpression of NOD-like receptor family CARD domain containing 5 (NLRC5) and intratumoral delivery of BO-112, a potent nanoplexed version of polyinosinic:polycytidylic acid (poly I:C) each restored the efficacy of ACT against B16-*Jak1*^{KO} tumors. Interestingly, BO-112 activated double stranded RNA (dsRNA) sensing (via protein kinase R and toll-like receptor 3) and induced MHC I expression via nuclear factor κB (NF-κB), independent of both IFN signaling and NLRC5. In summary, we demonstrated that in the absence of tumor IFN signaling, MHC I expression is essential and sufficient for the efficacy of ACT. For tumors lacking MHC class I expression as a result of deficient IFN signaling, activation of dsRNA sensors by BO-112 affords an alternative approach to restore the efficacy of tumor-specific CD8^{+} T cells.

Introduction

Intact tumor cell interferon (IFN) signaling was first identified as a critical piece of immune surveillance over two decades ago(*1, 2*). More recently, experience with immune checkpoint blockade has validated the importance of tumor cell-intrinsic IFN signaling to anti-tumor immune responses in patients(*3, 4*). Genetic or epigenetic disruption of tumor IFN signaling can result in primary or acquired resistance to immune checkpoint blockade(*5-8*).

In primary resistance to immune checkpoint blockade, tumor cell defects in IFN signaling disrupt adaptive expression of PD-L1 and negate the effects of targeting the PD1/PD-L1 axis(*9*). In acquired resistance, defects in IFN signaling render tumor cells insensitive to the positive effects of IFNs on antigen presentation and chemoattractant expression, and the negative effects of IFNs on cell proliferation. However, whether intact tumor IFN signaling regulates the direct cytotoxic capacity of a tumor-specific T cell is less clear. Upon engaging their target through recognition of the MHC-antigen complex, tumor-specific T cells release granzyme and perforin which induce apoptosis of the target cell(*10*). The role of tumor-intrinsic IFN signaling in this context is particularly relevant for adoptive cell therapy (ACT) approaches using tumor-specific T cells, such as T cell receptor (TCR)- or chimeric antigen receptor (CAR)-engineered T cell therapy.

To study the impact of tumor-intrinsic IFN signaling on the direct anti-tumor efficacy of tumor-specific T cells, we performed in vitro and adoptive transfer studies using tumor-specific T cells against a murine model of melanoma with IFN signaling defects (*Jak1* or *Jak2* loss) observed in patients with acquired resistance to immune checkpoint blockade. Only defects in *Jak1,* in which both type I and II tumor IFN signaling are disrupted, negated the efficacy of adoptively transferred tumor-specific T cells, a byproduct of the dependency of MHC class I expression on either type

I or II IFN signaling. This dependency could be circumvented genetically by overexpressing NLRC5, which upregulates MHC class I independent of an IFN signal(*11, 12*). As a pharmacologic approach, we utilized BO-112, a phase 1-tested, nanoplexed formulation of poly I:C, to uncouple tumor IFN signaling and MHC class I antigen presentation through activation of dsRNA sensing and NF-κB signaling, thereby restoring the efficacy of tumor-specific T cells.

Results

*B16-Jak1*KO *tumors are resistant to ACT due to deficiency in both type I and II IFN signaling*

To model the IFN signaling defects observed in human melanoma patients with primary or acquired resistance to immune checkpoint blockade, we generated *Jak1*KO and *Jak2*KO B16-F10 cell lines using CRISPR. As a functional validation of the CRISPR knockout cell lines, surface PD-L1 expression was evaluated in response to type I (IFNα, IFNβ) or type II (IFNγ) IFNs (Fig. 1A). Consistent with their aberrant signaling, B16-*Jak2*KO, and B16-*Jak1*KO tumors did not upregulate surface PD-L1 in response to type II, and either type I or II IFNs, respectively.

To evaluate the impact of defective tumor IFN signaling on response to immune checkpoint blockade in the B16 model, we combined anti-PD1 and anti-CTLA4 checkpoint blockade with focal radiation (RT, 12 Gy) in a dual flank tumor model, which results in a more robust anti-tumor immune response in the non-irradiated tumor than single or dual immune checkpoint blockade(*13, 14*). As expected, RT and dual checkpoint blockade resulted in a growth delay in the wildtype (WT) non-irradiated tumor ($p < 0.001$, multiple pairwise comparison); this effect was not observed in non-irradiated B16-*Jak2*KO or B16-*Jak1*KO tumors lacking type II IFN signaling, or both type I and II IFN signaling, respectively (Fig. 1B). The absence of type II

(*Jak2*KO) IFN signaling, or both (*Jak1*KO), did not impact the anti-tumor effects on the irradiated tumor (fig. S1).

To test the sensitivity of IFN signaling-deficient tumors to tumor-specific T-cells, we performed in vitro and adoptive transfer studies using T cells from pmel mice, which harbor a T-cell receptor transgene specific for gp100, a melanoma antigen highly expressed in B16 (Fig. 1C). B16 tumor cells retained gp100 expression after CRISPR modifications to IFN signaling pathways (fig. S2). Adoptive transfer of activated pmel T cells and IL-2 after lymphodepletion delayed the growth of wildtype tumors, compared to adoptive transfer of activated T cells from control C57BL/6 mice and IL-2 after lymphodepletion ($p < 0.01$, 2-way ANOVA; Fig. 1D). Adoptively transferred pmel T cells retained similar anti-tumor efficacy against B16-*Jak2*KO tumors deficient in type II IFN signaling. However, tumors lacking both type I and II IFN signaling (B16-*Jak1*KO) were completely resistant to the anti-tumor effect of pmel T cells. To evaluate whether tumor-intrisnic type I IFN signaling alone was responsible for the resistance to pmel T cells, we generated B16-*Ifnar1*KO tumors deficient in type I IFN signaling. The absence of type I IFN signaling did not impede the anti-tumor efficacy of adoptively transferred pmel T cells.

We modeled these in vivo findings using an in vitro coculture system, in which B16 wildtype or CRISPR modified tumor cells were pre-treated with either type I IFN (β) or type II IFN (γ), and subsequently exposed to either control or pmel T cells. Pre-treatment of wildtype B16 with either IFNβ or IFNγ sensitizes the tumor cells to killing by pmel T cells (Fig. 1E). Tumor cells pre-treated with an IFN for which the cognate signaling pathway was defective (B16- *Jak2*KO tumors pre-treated with IFNγ; B16-*Ifnar1*KO tumors pre-treated with IFNβ) were resistant to the cytotoxic effect of pmel T cells (Fig. 1E). B16-*Jak1*KO tumor cells were resistant to killing by pmel T cells despite pre-treatment with IFNβ or IFNγ (Fig. 1E). Based on these data, we concluded

that the in vivo sensitivity of B16 tumor cells to adoptively transferred pmel T cells is dependent on the activation of either type I or II IFN signaling. We hypothesized that this is related to the dependency of MHC class I expression on either type I or II IFN signaling.

Human melanoma exhibits IFN-dependent expression of MHC class I

IFN signaling is a well-described positive regulator of MHC class I antigen processing machinery(*15*). To better understand the role of IFN signaling in MHC I expression in melanoma, we evaluated the expression of MHC I in 48 human melanoma cell lines at baseline and in response to type I (IFNα, IFNβ) and type II IFN (IFNγ). Baseline MHC I expression in the human melanoma cell lines were distributed broadly, including a subset of cell lines with low baseline MHC I expression (Fig. 2A), similar to B16 murine melanoma (Fig. 1A). IFNα, IFNβ, and IFNγ each augment the surface expression of MHC class I ($p<0.0001$); an absolute increase in MHC I expression was observed in 85% (41/48), 92% (44/48), and 79% (38/48) of cell lines, respectively (Fig. 2A and fig. S3-4). The relative increase in MHC class I expression (MFI) in response to IFNγ was higher for cell lines in the lowest quartile of baseline MHC I expression, compared to the 2nd, 3rd or 4th quartiles (Fig. 2B). This pattern was recapitulated in response to IFNα and IFNβ (fig. S3-4), suggesting that MHC I expression exhibits greater IFN sensitivity in cell lines with low baseline MHC I expression.

We observed a similar IFN dependence of MHC class I expression in two previously reported patients with melanoma treated with anti-PD1 immune checkpoint blockade who developed acquired resistance due to a loss-of-function mutation in either *JAK1* or *JAK2(3)*. At baseline in the tumor from the patient who ultimately developed a *JAK1* loss-of-function

mutation, CD8+ T cell infiltration was observed at the invasive margin (as defined by S100 expression on human melanoma, Fig. 2C top panel). The S100+ melanoma cells at the invasive margin adjacent to CD8+ T cells expressed MHC I and PD-L1, in contrast to melanoma cells at a distance from the invasive margin. In contrast, at relapse in the *JAK1* mutant tumor, the S100+ melanoma cells in the *JAK1*-mutant tumor did not express MHC I and PD-L1; here, the MHC I and PD-L1 expression was limited to the margin surrounding the S100+ melanoma cells (bottom panel). In a second patient whose relapsed tumor harbored a *JAK2* loss-of-function mutation, a similar absence of MHC I expression was observed on S100+ melanoma cells, adjacent to an area of MHC I + stroma (Fig. 2D; baseline tumor not available). Together these clinical data support IFN dependence of MHC class I expression in patients with melanoma.

Nlrc5 overexpression bypasses IFN signaling to restore MHC I expression and sensitivity to tumor-specific T cells

We recapitulated the observed IFN dependency of MHC I expression in B16 murine melanoma. Consistent with their aberrant signaling, B16-*Ifnar1*KO, B16-*Jak2*KO, and B16-*Jak1*KO tumors did not upregulate surface MHC I in response to type I, type II, and both type I and II IFNs, respectively (Fig. 3A). To test the role of IFN dependence in vivo, we used B16 tumor cells overexpressing red fluorescent protein (RFP) and examined the expression of MHC I on CD45-RFP+ cells from tumor digests (fig. S5). RFP labeled B16-wildtype, B16-*Ifnar1*KO, and B16-*Jak2*KO tumor cells all expressed MHC I in vivo compared to the MHC I-deficient negative control (B16-*B2m*KO; Fig. 3B). However, B16-*Jak1*KO tumor cells did not express MHC I in vivo, indicating that either type I or II IFN signaling is necessary to induce MHC I expression on B16 tumor cells

in vivo. This contrasts with the patient presented in Figure 2B, where defect in type II IFN signaling alone was associated with an absence of MHC I expression.

To restore MHC I expression in IFN-deficient tumor cells, B16-*Jak1*^{KO} tumor cells were lentivirally transduced with *Nlrc5,* a transcriptional regulator of MHC I antigen processing machinery that has been shown to induce constitutive MHC I expression in wildtype B16 tumor cells(*11, 12*). Compared to those transduced with empty vector control, B16-*Jak1*^{KO}-Nlrc5 tumor cells expressed MHC I constitutively in the presence or absence of IFNγ (Fig. 3C). Forced expression of NLRC5 in the B16-*Jak1*^{KO} tumor cells rendered them sensitive to antigen-specific recognition by pmel T cells, as measured by IFNγ production in vitro (Fig. 3D). Likewise, forced expression of NLRC5 restored the sensitivity of B16-*Jak1*^{KO} tumors to adoptively transferred pmel T cells and IL-2 in vivo (Fig. 3E). However, overexpression of NLRC5 in wildtype B16 tumors did not augment the in vivo anti-tumor efficacy of adoptively transferred pmel T cells and IL-2 (fig. S6). These studies demonstrate that restoring surface expression of MHC I is critical for T cell recognition in the setting of loss-of-function mutations in genes affecting IFN signaling. Still, we do not exclude other potential MHC I independent functions for NLRC5 in the B16-Jak1^{KO} tumors.

BO-112 restores efficacy of tumor-specific T cells against tumors lacking type I and II IFN sensitivity

We reasoned that pharmacologic activation of pattern recognition receptor pathways may activate downstream signaling pathways redundant with IFN signaling, and in so doing, restore the efficacy of tumor-specific T cells against tumors with deficient IFN signaling and insufficient

MHC I expression. This would offer a pharmacological approach to upregulate MHC I expression in immunotherapy-resistant tumors with low baseline MHC I expression. To test this hypothesis, we used BO-112, a nanoplexed formulation of poly I:C administered intratumorally. In a phase 1 study, BO-112 was found to be safe as monotherapy or in combination with anti-PD1 immune checkpoint blockade in patients with solid tumors(*16*).

Intratumoral injection with BO-112, but not vehicle control, restored anti-tumor efficacy of adoptively transferred pmel T cells and IL-2 against B16-*Jak1*^{KO} tumors (Fig. 4A), similar to the effect of NLRC5 overexpression (compare with Fig. 3E). Of note, BO-112 also significantly augments the anti-tumor efficacy of adoptively transferred pmel T cells against wildtype B16 tumors, even though BO-112 is ineffective as monotherapy ($p<0.05$, fig. S7). To evaluate the contribution of adoptively transferred and endogenous immune cells to the anti-tumor response, we performed parallel bulk RNAseq and single cell mass cytometry of tumor specimens five days after ACT. By RNAseq, the samples clustered by treatment group (control T cells and vehicle, control T cells and BO-112, pmel T cells and vehicle, pmel T cells and BO-112) on principal component analysis (PC1, PC3; Fig. 4B). Compared to B16-*Jak1*^{KO} tumors treated with control T cells and intratumoral vehicle injection, 700 transcripts were uniquely upregulated in tumors treated with pmel T cells and intratumoral BO-112 (hereafter referred to as the pmel-BO-112 gene set; Fig. 4C). Although we did not observe an increase in CD8 pmel T cell infiltration in the samples treated with pmel T cells and BO-112 compared to samples treated with pmel T cells and vehicle using single cell mass cytometry (fig. S8), the pmel-BO112 gene set was strongly correlated with infiltration of adoptively transferred CD8 pmel T cells, but not endogenous T cells (Fig. 4D). Endogenous myeloid populations, in particular granulocytic MDSCs (PMN-MDSCs) and tumor-associated macrophages (TAMs), were also associated with

expression of the pmel-BO-112 gene set. We cannot exclude that these other cells contribute to a coordinated anti-tumor immune response in the group treated with pmel T cells and BO-112.

To further evaluate whether the impact of BO-112 on the anti-tumor efficacy in the IFN-deficient B16-*Jak1*KO tumor model was dependent on recognition of tumor cells by pmel T cells via MHC I, we generated a B16-*B2m*KO tumor that lack surface MHC class I due to a defect independent of IFN signaling. Like B16-*Jak1*KO tumors, B16-*B2m*KO tumors are also resistant to pmel T cells even after pretreatment with IFNγ (fig. S9). However, unlike its effect on B16-*Jak1*KO tumors, BO-112 did not restore the anti-tumor effect of adoptively transferred pmel T cells against B16-*B2m*KO tumors (Fig. 4E).

BO-112 induces MHC I expression in an IFN- and Nlrc5-independent manner in murine and human melanoma

Upon exposure in vitro, BO-112 augmented the expression of surface MHC I and PD-L1 on wildtype B16 cells, similar to the effects of type I and II IFNs (Fig. 5A and 5B, top panels). However, only BO-112, but not type I or type II IFNs, augmented the expression of the B16-*Jak1*KO cell line (Fig. 5A and 5B, bottom panels). Expression of MHC I antigen processing machinery genes *B2m and Tap1* were augmented within 6 hours of exposure to BO-112 (Fig. 5C). Furthermore, tumor-specific IFNγ production by pmel T cells occurred after pre-treatment of wildtype B16 tumor cells with either BO-112 or IFNγ. In contrast, pmel T cells only recognized B16-*Jak1*KO tumor cells pre-treated with BO-112, but not IFNγ (Fig. 5D). We also evaluated the induction of MHC I by BO-112 in two human melanoma cell lines CRISPR-modified with defects in IFN signaling, M202-*JAK1*KO and M407-*JAK1*KO, as well as three human melanoma cell lines

with low basal MHC I expression that was not inducible by IFNγ (M311, M368 and M412B; Fig. 2A). BO-112 augmented surface MHC I expression in all cell lines except M311 (Fig. 5E).

Given the importance of *Nlrc5* in coordinating the expression of MHC I antigen processing machinery, and its position downstream of IFN signaling, we considered that the effect of BO-112 on MHC I expression may occur through induction of *Nlrc5* expression. Indeed, BO-112 augments the expression of *Nlrc5* in both wildtype B16 and B16-*Jak1*^{KO} tumor cells (fig. S10). To test the functional role of *Nlrc5* in MHC I expression induced by BO-112, we generated two different B16-*Nlrc5*^{KO} tumor cell clones and two different B16-*Jak1*^{KO}-*Nlrc5*^{KO} tumor cell clones by CRISPR. As anticipated, MHC I induction by IFNγ was greatly diminished in B16-*Nlrc5*^{KO} tumor cells compared to wildtype B16 (fig. S10). However, MHC I induction by BO-112 was retained in both B16-*Nlrc5*^{KO} and B16-*Jak1*^{KO}-*Nlrc5*^{KO} tumor cells (Fig. 5F and Fig. S10). Thus, MHC I induction by BO-112 occurs in both an IFN- and *Nlrc5*-independent manner.

The BO-112 nanoplexed formulation of poly I:C was designed to engage double stranded RNA (dsRNA) sensors. We compared the MHC I augmenting effects of BO-112 with the effects of a standard formulation of poly I:C, as well as two other pattern recognition receptor (PRR) agonists (lipopolysaccharide (LPS), a TLR4 agonist, and CpG oligonucleotides, which activate TLR9) to determine whether the effect on antigen presentation was specific to BO-112 or broadly applicable to PRR agonists. In a mouse macrophage cell line (RAW 264.7) known to respond to PRR agonists(*17*), LPS, CpG, poly I:C all resulted in an increase in MHC I expression, as did BO-112. However, aside from BO-112, none of the PRR agonists augmented MHCI expression of the wildtype B16 or B16-*Jak1*^{KO} cell lines (Fig. 5G). The surface MHC I expression of the IFN-insensitive M202-*JAK1*^{KO} human melanoma cell line increased in response to both poly I:C and BO-112, but neither LPS nor CpG, suggesting an effect unique to dsRNA sensing (Fig. 5H).

BO-112 bypasses IFN signaling to induce MHC class I expression through activation of NF-κB signaling

RNA-sequencing analysis of the B16-*Jak1*KO tumor cell line six hours after treatment with vehicle or BO-112 revealed a set of 190 genes differentially expressed in response to BO-112 ($p<0.01$, FDR<0.05, and Log_2(Fold Change)>1.5; Fig. 6A, left panel). Gene set enrichment analysis was used to identify differentially expressed gene sets ($p<0.01$, $q<0.05$, normalized enrichment score>1.5) that contained at least 30 genes that were also differentially expressed, identifying 8 significantly different gene sets that were upregulated in BO-112-treated B16-*Jak1*KO cells, compared to vehicle-treated B16-*Jak1*KO (Fig. 6A), right panel. Despite the absence of IFN signaling in B16-*Jak1*KO tumor cells, BO-112 induces an "IFN-like" gene signature, highlighted by genes in the Hallmark IFN Gamma Response Pathway, the Hallmark IFN Alpha Response Pathway and the Reactome IFN Signaling gene sets. Importantly, to determine whether the tumor-intrinsic effects of BO-112 in vitro were also observed in vivo, we examined the genes that were specifically upregulated in B16-*Jak1*KO tumors, treated with BO-112 and either pmel or control T cells (135 genes; Fig. 6B). Of these 135 genes, 55 were significantly increased both in vitro and in vivo in groups treated with BO-112 (Fig. 6B, $p<0.01$, FDR<0.05, and Log_2(Fold Change)>1.5). Notably, 23 of these 55 genes were involved in either type I IFN signaling or TNF-α signaling via NF-κB (Fig. 6C).

We postulated that NF-κB could be the transcriptional effector of the signaling induced by BO-112 that was responsible for IFN- and *Nlrc5*-independent MHC I expression. Indeed, treatment with BO-112 augmented cytoplasmic phosphorylation and nuclear translocation of NF-κB (p65) (fig. S11). We treated our B16- *Jak1*KO cell line with BO-112 in conjunction with a

selective NF-κB inhibitor, BMS-345541. BMS-345541 abrogated the induction of MHC I by BO-112 in a dose-dependent manner (Fig. 7A). A transient knockdown of *Rela* via two different siRNAs achieved a similar effect, inhibiting the upregulation of surface MHC I by BO-112 in B16-*Jak1*KO tumors, as well as human melanoma M407-JAK1KO (Fig. 7B).

We screened the effects of siRNA targeting four putative dsRNA sensors on induction of MHC I by BO-112. Knockdown of *Pkr* and *Tlr3*, both of which are known to directly signal through NF-κB(*18-20*), but not *Ifih1* or *Ddx58* , abrogated MHC I induction by BO-112 (Fig. 7C, fig. S12). Of these, only siRNA against PKR completely abrogated the effect of BO-112 on MHC I induction. Consistent with the hypothesis that BO-112 activates NF-κB signaling via PKR, siRNA targeting PKR reduced the abundance of nuclear NF-κB (p65) in response to BO-112 (Fig. 7D).

Discussion

Although immune checkpoint blockade is effective in a subset of patients with melanoma and other malignancies, most patients still do not benefit. Tumor defects in IFN signaling are an important mechanism of both primary and acquired resistance to immune checkpoint blockade(*3, 4, 6, 8, 21*). This role of IFN signaling is consistent with classical preclinical studies that demonstrated the importance of tumor IFN sensitivity in mounting an effective anti-tumor immune response(*1, 2*). Accordingly, we observed resistance to the combination of dual immune checkpoint blockade and focal radiation in B16 murine melanoma with defects in *Jak1* or *Jak2* observed in patients with acquired resistance to immune checkpoint blockade.

We queried whether T cell-based ACT could be an effective approach to overcome resistance in tumors with defective IFN signaling, especially given the increased utilization of ACT with

tumor-infiltrating lymphocytes (TIL) and T cell receptor (TCR) or chimeric antigen receptor (CAR) engineered T cells for patients with cancer. Notably, the efficacy of ACT with tumor-specific pmel T cells was unaffected by defects in *Jak2* or *Ifnar1* in B16 tumors. However, ACT with pmel T cells was ineffective against B16-*Jak1*^{KO} tumors lacking both type I and II IFN signaling both in vitro and in vivo.

Our findings indicate that either type I or II IFN signaling is necessary to coordinate MHC I antigen presentation by B16 tumor cells in vivo, and thereby confer sensitivity to pmel ACT. The role of IFN signaling in the coordinated expression of MHC I antigen processing machinery (including peptide processing and transportation) is well-described(*15, 22*), and melanoma tumors with defective MHC I expression and IFN signaling have been reported(*4*). MHC I expression on B16 is known to be absent in vitro at baseline, and readily inducible by IFN(*23, 24*). This phenotype of low basal and IFN-inducible MHC I expression is not unique to B16 murine melanoma. While human melanoma cell lines have variable expression of MHC I, we found that a subset can also exhibit poor basal expression of MHC I that can be induced by type I or II IFNs. And in relapsed tumors from patients after anti-PD1 immune checkpoint blockade with absent IFN signaling, the putative IFN-dependent gradient of MHC I expression at the tumor margin was no longer observed. Others have also reported that melanoma lesions progressing in the context of immune-based therapies have weak MHC I expression(*25, 26*).

We used NLRC5 as a tool to restore constitutive MHC I expression in the IFN signaling-deficient B16-*Jak1*^{KO} model, and in doing so restored the anti-tumor efficacy of pmel ACT. Thus, when MHC I is constitutively expressed, the absence of tumor IFN signaling does not negate the efficacy of tumor-specific CD8+ T cells. This is consistent with the capacity of effector T cells to

directly kill tumor cells in a perforin and granzyme dependent manner, independent of IFN signaling(*10*).

Our findings also highlight the different mechanisms that drive resistance to immune checkpoint blockade and ACT. IFN signaling has diverse downstream effects, including direct anti-proliferative effects(*27, 28*), the induction of immune checkpoints such as PD-L1(*29, 30*), the expression of T cell chemoattractants CXCL9 and CXCL10(*31-33*), and the coordinated expression of antigen presentation machinery. In the context of immune checkpoint blockade, the complex interplay of each of these factors may drive response or resistance(*9*). In some model systems, defects in IFN signaling have even resulted in improved efficacy of immune checkpoint blockade(*14, 34*). In other scenarios, antigen presentation can be defective despite intact IFN signaling(*35*). In the context of T cell-based ACT, our results suggest that the role of tumor IFN signaling is primarily tied to its effect on antigen presentation. From this we infer also that CAR T cells, which target tumors independent of MHC expression, would also be effective against interferon-deficient tumors.

In the absence of IFN signaling, alternative means to induce MHC I expression are needed. BO-112 is a nanoplexed formulation of poly I:C that activates dsRNA sensors such as TLR3, MDA5, RIG-I and PKR. When administered intratumorally in phase 1 studies in combination with anti-PD1 immune checkpoint blockade, BO-112 can induce clinical responses in patients refractory to anti-PD1 therapy alone(*16*). We found that BO-112 can induce MHC I expression in IFN signaling-deficient melanoma, and thus restore the anti-tumor activity of pmel ACT. However, BO-112 restored MHC I expression through an NF-κB mediated mechanism and independent of NLRC5. NF-κB is a known regulator of MHC class I expression, especially at the HLA-A locus(*36-38*) and is directly activated by dsRNA sensors TLR3(*20*) and PKR(*18, 19*).

Interestingly, among canonical dsRNA sensors, *Pkr* and *Tlr3* mediated the effect of BO-112 on MHC I in B16 melanoma. These findings are consistent with the capacity of West Nile virus, a single-stranded RNA virus, to induce MHC I in mouse embryonic fibroblasts in an NF-κB - dependent and IFN-independent manner(*39*).

There is also emerging literature on the role for tumor cell intrinsic dsRNA sensing in response and resistance to immunotherapy. Tumor cell intrinsic dsRNA sensing via RIG-I was illustrated to be critical for response to immune checkpoint blockade, though in IFN replete models(*40*). As another example, loss of ADAR1 in B16 tumor cells, for example, amplified dsRNA sensing and sensitized B16 tumors to anti-PD1 and GVAX immunotherapy(*41*). Our findings illustrate a mechanism by which dsRNA sensing can restore sensitivity to T cell-based ACT.

Our study has limitations. First, our modeling does not account for the resistance of patients harboring tumors with sufficient basal levels of MHC I expression despite tumor-intrinsic IFN defects. And while we demonstrated that BO-112 can also augment the efficacy of ACT against tumors with low MHC I expression that retain IFN sensitivity, the contribution of IFN-independent MHC I induction is less likely a major factor in this context. Second, the direct effects of BO-112 on tumor cells is limited to injected lesions. Systemic delivery of a tumor-specific dsRNA agonist may maximize the therapeutic potential of this approach. Third, while we used JAK1 and JAK2 knockout models to model IFN insensitivity, these kinases are also involved in pathways other than IFN signaling. To address this, we conducted studies utilizing IFN- α, -β, and/or -γ as stimuli to highlight the specific role of IFN signaling in each knockout model.

In conclusion, we propose that T cell-based ACT can still be an effective immunotherapy approach in tumors with JAK2 loss that are resistant to immune checkpoint blockade, so long as there is sufficient antigen presentation. In the absence of IFN-inducible antigen presentation,

such as in tumors with JAK1 loss, activation dsRNA pattern recognition receptor sensors by BO-112 provides an IFN-independent approach to restore MHC I expression via NF-κB and sensitize tumors to the direct anti-tumor effect of CD8+ T cell-based ACT.

Materials and Methods

Study Design We examined the effect of tumor-intrinsic defects in IFN signaling on the anti-tumor efficacy of tumor-specific T cells. We used syngeneic mouse melanoma cell lines (B16-F10) with CRISPR-generated deficits in either type I, type II or both type I and II IFN signaling. Treatments included tumor-specific pmel T cells (or tumor non-specific C57BL/6 T cells as a control) and BO-112, a nanoplexed formulation of poly I:C delivered intratumorally (or its vehicle as a control). We performed in vivo adoptive cell transfer studies and in vitro coculture experiments, and measured tumor growth, activation of T cells, and gene and protein expression. Mice were randomized to treatment groups after tumors were established to ensure consistent tumor sizes. Number of mice per group and statistical analysis is described in more detail in the figure legends and statistical methods. In cases where an outlier tumor was identified by size prior to initiation of treatment (Grubbs' test), this tumor was excluded from analysis. Tumors were measured by an individual blinded to treatment groups. In vivo experiments are representative of at least two replicates. For in vitro experiments, biological duplicates or triplicates were tested, and experiments are representative of at least two replicates.

Cell Lines The B16-F10 mouse melanoma cell line and RAW264.7 were purchased from ATCC. B16-F10, RAW264.7 and patient-derived human melanoma cell lines were cultured with complete medium (RPMI 1640 with L-glutamine, Fisher Scientific) containing 10% fetal bovine serum (Omega Scientific), penicillin (100 U/mL, Omega Scientific), streptomycin (100 μg/mL, Omega Scientific), and amphotericin B (0.25 μg/ml, Omega Scientific). Mouse T cells were cultured in complete media supplemented with 10% fetal bovine serum (Hyclone Characterized Fetal Bovine Serum), antibiotics, and 50 uM 2-mercaptoethanol (Gibco). Cell lines were confirmed mycoplasma negative using mycoplasma detection kit (Biotool #B3903), and

periodically tested for authentication. For in vivo experiments, early passage cell lines were used (less than ten passages).

Animals Mice were bred and kept under defined-flora, pathogen-free conditions at the Association for the Assessment and Accreditation of Laboratory Care-approved animal facility of the Division of Experimental Radiation Oncology, University of California, Los Angeles (UCLA) and used under a UCLA Animal Research Committee approved protocol. Pmel-1 TCR/Thy1.1 transgenic mice on a C57BL/6 background were obtained from the Jackson Laboratory.

CRISPR/Cas9 knockout For human melanoma cell lines M407 and M202, CRISPR/Cas9 mediated knockouts of *JAK1* were generated as previously described(*3*). For mouse cell lines, CRISPR/Cas9 gene targeting was accomplished by first cloning the guide sequence (selected using the CRISPOR program) into the pSpCas9(BB)-2A-GFP vector (Addgene) containing an ampicillin resistance gene (*42*). The sequences for each guide used are listed in **table S1**. DNA was isolated from Transformed One Shot Stbl3 Chemically Competent E. coli (Invitrogen) colonies selected by ampicillin resistance, and verified using a U6 promoter primer forward 5-GCCTATTTCCCATGATTCCTTC–3. Mouse tumor cell lines were transfected using Lipofectamine 3000 reagent (Fisher) and single cell sorted from the bulk population by GFP expression (Aria II BD Biosciences). Expanding clones were screened for successful CRISPR modification using targeted PCR amplification of the sgRNA target region (HotStarTaq Master Mix, QIAGEN), followed by Sanger sequencing. Successful targeting of genes of interest was determined by tracking of indels by decomposition (TIDE) analysis (Netherlands Cancer Institute, NKI; https://tide.nki.ni). CRISPR knockouts of genes responsible for IFN signaling (*Jak1, Jak2, Ifnar1)* were further confirmed by functional assessment of surface MHC I and PD-L1 expression in response to IFNs (Fig. 1A). CRISPR knockout of *B2m* was confirmed by surface

MHC I expression after IFN-treatment. As a control cell line for the CRISPR process, we used a wildtype B16 clone (B16-WT) in which targeting of the genes of interest was unsuccessful (B16-WTCC).

Evaluation of Surface MHC I and PD-L1 Expression Cell lines were seeded in complete media containing 100 ng/mL of IFNγ (Peprotech, Cat# 315-05), 500 IU/mL of IFNβ (Merck Millipore, Cat# IF011), 500 IU/mL of IFNα (Merck Millipore, Cat# IF009), 0.5-1.0 μg/mL BO-112 (Highlight Therapeutics), BMS-345541 (Sigma-Aldrich), or PBS for 18 hours. In other experiments, cells were treated with 100 ng/mL LPS (Invivogen, #tlrl-b5lps), 10 μg /mL CpG ODNs (Invivogen, #tlrl-1826), or 100 μg/mL poly I:C (Invivogen, #tlrl-pic). After 18 hours, cells were harvested with 10 mM EDTA (Sigma-Aldrich) and surface-stained in phosphate-buffered saline (PBS), 5% fetal bovine serum, and 2 mM EDTA with allophycocyanin (APC) anti-mouse H-2K^b (Biolegend #116518, clone AF6-88.5) and phycoerythrin (PE) anti-mouse PD-L1 (Biolegend #155404, clone MIH7) for murine tumor cells, and with PE-Cy7 anti-human HLA-A,B,C (Biolegend #311430, clone W6/32) and APC anti-human PD-L1 (Biolegend #374514, clone MIH3) for human tumor cells. Cells were analyzed by flow cytometry using a LSRII (BD Biosciences). Data was analyzed using the FlowJo software (version 10.6.1).

Generation of tumor-specific murine T cells Splenocytes from pmel transgenic mice were cultured in T cell media plus murine IL-2 (Peprotech), and pulsed with murine gp100 peptide (Fisher). C57BL/6 mice were used as a control, and splenocytes were cultured in T cell media, murine IL-2 (Peprotech), and pulsed with anti-CD3 and anti-CD28 antibodies. Expanded T cells were then washed and cultured in murine IL-2 and used for in vivo adoptive cell transfer or in vitro coculture experiments between day 3 and day 9.

Tumor Cell Proliferation Assay Cell lines were transduced with a nuclear localizing RFP (NucLight Red Lentivirus EF1a Reagent, Essen Biosciences) to facilitate cell counts. B16-WT and knockout cell lines (RFP_+) were pulsed with 100 ng/mL of IFNγ and 500IU/mL of IFNβ 18 hours before coculture, and 0.5 μg /mL of BO-112 (Highlight Therapeutics) six hours before coculture. After 18 hours, RFP_+ murine melanoma cells were harvested using 10mM EDTA and plated in a flat bottom 96-well plate in triplicate for each condition at 5000 cells per well for IncuCyte Live Cell Analysis (Essen Bioscience). Pmel-1 T-cells and C57BL/6 splenocytes were added at 2:1 effector to target ratio. At least two phase-contrast and fluorescent images were obtained of each well every two hours using the IncuCyte live imaging system for at least 72 hours. Images were quantified by percentage confluence of the fluorescent signal.

ELISA B16-WT and knockout cell lines (RFP_-) were pulsed with 100 ng/mL of IFNγ and 500 IU/mL of IFNβ 18 hours before coculture, and 0.5 μg /mL of BO-112 six hours before coculture. Target tumor cells were harvested using 10 mM EDTA and plated in a round bottom 96-well plate in triplicate for each condition at 100,000 cells per well. Pmel-1 T-cells and C57BL/6 splenocytes were added at 1:1 effector to target ratio. The cocultured cells were incubated at 37˚C for 24 hours. Supernatant was then harvested and frozen at -20˚C. Coculture supernatants were thawed and analyzed by ELISA for mouse IFNγ (ThermoFisher) according to the manufacturer's instructions.

Gene Expression Assays Total RNAs were extracted using the PureLink RNA Mini Kit (Invitrogen) or RNeasy mini kit (Qiagen). Gene expression was then measured using the Power SYBR Green RNA-to-CT 1-Step Kit (ThermoFisher) according to the manufacturer's instructions. RT-PCR was performed with the ViiA 7 Real-Time PCR System (ThermoFisher). Data was normalized by 18s expression.

Immunohistochemistry Tumor samples were obtained and slides were stained as previously described (*3*). Briefly, staining was performed at the UCLA Translational Pathology Core Laboratory using Leica Bond ancillary reagents and REFINE polymer DAB detection system. Briefly slides were stained with S100 (Dako, Carpinteria, CA), CD8 (Dako), PD-L1 (clone SP142, Spring Bio), and MHC Class I (clone HC 10, Saphirre NA) and scanned at 40X on an Aperio ScanScope AT (Leica Biosystems).

Murine NLRC5 plasmid design Total RNA was obtained from murine splenocytes using the PureLink RNA Mini Kit (Invitrogen) according to the manufacturer's instructions. Total RNA was then reverse transcribed to cDNA using the Superscript IV Reverse Transcriptase Kit (ThermoFisher) with an Oligo(dT)20 primer (ThermoFisher). The cDNA was then amplified using the Phusion High-Fidelity PCR Kit (New England BioLabs) and primers specific for the NLRC5 coding sequence. A Gibson Assembly (New England BioLabs) kit was used to incorporate the NLRC5 PCR product into the pRRL-MSCV viral plasmid and confirmed by Sanger sequencing.

Lentiviral vector production and gene transfer Lentivirus was achieved by co-transfection of 293T cells (ATCC). Poly-L-lysine (Sigma Aldrich) coated tissue culture plates were seeded with 5x10^6 293T cells and allowed to adhere. Media was then replaced with complete media without FBS. Cells were transfected with pRRL-MSCV-mNLRC5 (5 μg) or pRRL-MSCV-mGFP (5 μg), along with pCMV8.9 (5 μg), and pCAGGS-VSV-G (1 μg) using TransIT-293 Transfection Reagent (MirusBio). After 17 hours, the media was replaced with DMEM medium with 10% fetal bovine serum containing 20 mM HEPES (Invitrogen) and 10 mM Sodium Butyrate (Sigma Aldrich). After eight hours, cells were washed and replenished with complete DMEM medium with 20 mM HEPES. After 24 hours, the supernatants were collected, filtered through 0.45 uM filters, and stored at -80˚C. For transduction, B16-WT and B16-*Jak1*KO tumor cells at 40-60%

confluence were incubated with viral supernatant along with 8μg/mL of polybrene (Sigma Aldrich). After 12-16 hours, media was replaced and cells were expanded and sorted (Aria II, BD Biosciences) based on augmented basal expression of MHC I.

In Vivo Adoptive Cell Therapy Studies B16-WT or CRISPR-modified cells ($5x10^5$) were injected subcutaneously in the right flank of C57BL/6 mice (6-10 weeks of age). Female mice were used to match the sex of the pmel mice from which adoptively transferred T cells were derived. Seven days after tumor inoculation, mice were treated with lymphodepleting (500 cGy) total body irradiation. On day 9, $4.0\text{-}5.0x10^6$ gp100-activated pmel-1 T cells (or control BL/6 T cells) were adoptively transferred (intravenously) to mice bearing palpable tumors (~50 mm^3). Mice were also treated with recombinant human IL-2 (50,000 IU per day, intraperitoneal) for 3 consecutive days starting on the day of adoptive transfer. Beginning the day after adoptive transfer, BO-112 was administered via intratumoral injection at 2.5 mg/kg, twice a week for a total of three doses. Tumor size (*length x width)* was monitored every two to three days and volume was calculated as (*length x* $width^2$*)/2)*.

In Vivo Immune Checkpoint Blockade Studies B16-WT or CRISPR-modified cells ($5x10^5$) were injected subcutaneously in bilateral flanks of ($5x10^5$) C57BL/6 mice (6-10 weeks of age) on day 0. When tumors reached a volume of at least 50 mm^3, mice were randomized into different groups of treatment according to the experimental plan. InVivoMab anti-mouse PD1 (Ref# BE0146) and anti-mouse CTLA4 (Ref# BE0131) or their corresponding isotypes, anti-trinitrophenol (Rat IgG2a, Ref# BE0089) and polyclonal Syrian hamster IgG (Ref# BE0087) from BioXCell were administered by intraperitoneal injection (200μg/antibody/dose). Focal tumor-directed computed tomography-guided radiation was delivered using the Small Animal Radiation Therapy platform (Precision Xray) with mice anesthetized using isoflurane. Tumors were

measured daily until the animals died or the tumor volume reached 2000mm^3.

siRNA experiments Cells were plated in triplicates for each siRNA condition. After 8 hours, cells were transfected with scrambled or on-target siRNAs (see **table S2)** using Lipofectamine RNAiMAX (ThermoFisher cat# 13778150) according to manufacturer's guidelines. Alternatively, cells were transfected with ON-TARGET Plus siRNA Pools for PKR or Non-targeting Control (siNTC) (Dharmacon). After 48-72 hours of transfection, media was replaced with fresh media containing either 0.5 μg /mL BO-112 (Highlight Therapeutics) or vehicle (5% glucose in PBS). After six or 18 hours, cells were harvested with 10 mM EDTA in PBS and analyzed by flow cytometry or harvested for downstream protein analysis by Western Blot.

Western Blot Nuclear and cytoplasmic protein fractions were obtained by using NE-PER Nuclear and Cytoplasmic Extraction Kit (Pierce) according to manufacturer's instructions. Antibodies are listed in **table S2.**

Mass and Flow cytometry of In Vivo Tumor Specimens Single cell suspension of tumors harvested from mice were stained as previously described(*43*). Briefly, tumors were minced and dissociated using a murine tumor dissociation kit (Miltenyi Biotec cat#130-096-730) and a gentleMACS Octo Dissociator (Miltenyi Biotec cat# 130-095-937). Cells were then resuspended in PBS and filtered through a 70 um cell strainer to obtain single cell suspensions. For mass cytometry, the single cells were first stained with Cell-ID Cisplatin (1:2500 dilution, Fluidigm cat# 201064) for 5 minutes at 37C. Cells were then washed with PBS and stained with the surface antibody cocktail for 30 mins at RT. Cells were again washed and fixed with 1.6% Formaldehyde for 20 minutes at RT. After fixation, cells were then washed with Maxpar Perm-S Buffer (Fluidigm cat# 201066) and stained with the intracellular antibody cocktail for 30 minutes at RT. Finally, cells were stained with the intercalating solution (Cell-ID Intercalator-Ir, cat#201192B) at a

1:6000 dilution in Maxpar Fix and Perm Buffer (Fluidigm cat# 201067) overnight at 4C. For flow cytometry experiments, cells were stained first in PBS with viability dye (Zombie-UV Fixable Viability Kit, Biolegend cat#423107), and then washed and stained with surface antibodies in PBS, 5% fetal bovine serum, and 2 mM EDTA. Antibodies are listed in **table S2.** Data were acquired using the Fluidigm Helios mass cytometer or LSRII (BD Biosciences) flow cytometer. For mass cytometry data, manually gated CD45+ populations (FlowJo software, version 10.4.2) were analyzed using Cytofkit package (R version 3.5.1). Dimensionality reduction using t-SNE algorithm was performed on each data set, and plots were generated by PhenoGraph clustering through cytofkiyShinyAPP from Cytofkit(*44*). Flow cytometry data was analyzed in FlowJo software (version 10.6.1).

RNA sequencing and analysis: Murine subcutaneous tumors were harvested and stored in RNA later overnight at 4˚C before transferring to -80˚C. Total RNA was extracted from tumors or cell lines using the AllPrep DNA/RNA Micro Kit (Qiagen). RNA sequencing (RNAseq) libraries were prepared using the KAPA mRNA stranded library preparation kit, according to the manufacturer's recommendations. Libraries were pooled and sequenced on the Illumina HiSeq3000 platform (50 bp reads). Reads were aligned to the mouse reference genome (mm9/GRCm38) using HISAT2 (v2.0.4)(*45*). Gene expression was quantified using HTSeq-counts (v0.6.1)(*46*). Differential expression analysis was performed using DESeq2(*47*), and subsequent gene set enrichment analysis was performed using the fgsea(*48*) and msigdbr(*49*) R packages, specifically on the Hallmark, KEGG, and REACTOME annotated gene sets. Differentially expressed genes and gene sets were filtered to those with a p value of less than 0.05 and a Benjamini-Hochberg corrected FDR value less than 0.25. Gene expression was visualized using the Z score of normalized gene expression (calculated using the variance-

stabilizing transform from DESeq2) using the ggplot2 R package(*50*). Gene expression was correlated with the mass cytometry data by calculating the Pearson correlation coefficient between the normalized gene expression (calculated using the variance-stabilizing transform from DESeq2) and the relative percentages of each cell type (of total CD45+ cells) as determined by Cytofkit (described above). Genes most highly correlated with cell types were filtered by those with a Pearson correlation of at least 0.5.

Statistical analysis and reproducibility

Prism (versions 7 and 8) software (GraphPad) was utilized to analyze differences between groups and determine statistical significance; $p<0.05$ was considered statistically significant. Normality assumption was evaluated for outcomes before statistical testing. For in vitro studies, including tumor growth, surface protein expression, gene expression, and cytokine production, as well as in vivo tumor growth studies, differences between groups were evaluated using two-sided unpaired *t* tests. For in vivo studies, tumor growth is shown as mean +/- standard error of the mean (SEM). Differences in mouse survival between treatment groups were evaluated using the log-rank test. Statistical analysis of RNA sequencing data is described above.

List of Supplementary Materials:

REFERENCES AND NOTES

1. D. H. Kaplan *et al.*, Demonstration of an interferon gamma-dependent tumor surveillance system in immunocompetent mice. *Proceedings of the National Academy of Sciences of the United States of America* **95**, 7556-7561 (1998).
2. A. S. Dighe, E. Richards, L. J. Old, R. D. Schreiber, Enhanced in vivo growth and resistance to rejection of tumor cells expressing dominant negative IFN gamma receptors. *Immunity* **1**, 447-456 (1994).
3. J. M. Zaretsky *et al.*, Mutations Associated with Acquired Resistance to PD-1 Blockade in Melanoma. *The New England journal of medicine* **375**, 819-829 (2016).
4. A. Sucker *et al.*, Acquired IFNgamma resistance impairs anti-tumor immunity and gives rise to T-cell-resistant melanoma lesions. *Nature communications* **8**, 15440 (2017).
5. S. J. Patel *et al.*, Identification of essential genes for cancer immunotherapy. *Nature* **548**, 537-542 (2017).
6. R. T. Manguso *et al.*, In vivo CRISPR screening identifies Ptpn2 as a cancer immunotherapy target. *Nature* **547**, 413-418 (2017).
7. D. Pan *et al.*, A major chromatin regulator determines resistance of tumor cells to T cell-mediated killing. *Science (New York, N.Y.)* **359**, 770-775 (2018).
8. D. S. Shin *et al.*, Primary Resistance to PD-1 Blockade Mediated by JAK1/2 Mutations. *Cancer discovery* **7**, 188-201 (2017).
9. A. Kalbasi, A. Ribas, Tumour-intrinsic resistance to immune checkpoint blockade. *Nat Rev Immunol*, (2019).
10. I. Voskoboinik, J. C. Whisstock, J. A. Trapani, Perforin and granzymes: function, dysfunction and human pathology. *Nat Rev Immunol* **15**, 388-400 (2015).
11. T. B. Meissner *et al.*, NLR family member NLRC5 is a transcriptional regulator of MHC class I genes. *Proceedings of the National Academy of Sciences* **107**, 13794-13799 (2010).
12. G. M. Rodriguez *et al.*, NLRC5 elicits antitumor immunity by enhancing processing and presentation of tumor antigens to CD8(+) T lymphocytes. *Oncoimmunology* **5**, e1151593 (2016).
13. C. Twyman-Saint Victor *et al.*, Radiation and dual checkpoint blockade activate non-redundant immune mechanisms in cancer. *Nature* **520**, 373-377 (2015).
14. J. L. Benci *et al.*, Tumor Interferon Signaling Regulates a Multigenic Resistance Program to Immune Checkpoint Blockade. *Cell* **167**, 1540-1554.e1512 (2016).
15. D. P. King, P. P. Jones, Induction of Ia and H-2 antigens on a macrophage cell line by immune interferon. *Journal of immunology (Baltimore, Md. : 1950)* **131**, 315-318 (1983).
16. L. F. Rodas IM, Rodriguez-Ruiz M, Calles A, Perez-Gracia JL, Gomez-Rueda A, Lopez-Tarruella S, Ponz-Sarvise M, Alvarez RM, Soria A, de-Miguel E, Gayarre J, Aznar MA, Calvo A, Lopez-Casas PP, Tersago D, Quintero M, Martin-Algarra S, Martin M, Melero I. , in *ESMO* (Munich, 2018).
17. H. Hacker *et al.*, Immune cell activation by bacterial CpG-DNA through myeloid differentiation marker 88 and tumor necrosis factor receptor-associated factor (TRAF)6. *The Journal of experimental medicine* **192**, 595-600 (2000).
18. M. C. Bonnet, R. Weil, E. Dam, A. G. Hovanessian, E. F. Meurs, PKR stimulates NF-kappaB irrespective of its kinase function by interacting with the IkappaB kinase complex. *Mol Cell Biol* **20**, 4532-4542 (2000).

19. M. Zamanian-Daryoush, T. H. Mogensen, J. A. DiDonato, B. R. Williams, NF-kappaB activation by double-stranded-RNA-activated protein kinase (PKR) is mediated through NF-kappaB-inducing kinase and IkappaB kinase. *Mol Cell Biol* **20**, 1278-1290 (2000).
20. Z. Jiang, T. W. Mak, G. Sen, X. Li, Toll-like receptor 3-mediated activation of NF-kappaB and IRF3 diverges at Toll-IL-1 receptor domain-containing adapter inducing IFN-beta. *Proceedings of the National Academy of Sciences of the United States of America* **101**, 3533-3538 (2004).
21. J. Gao *et al.*, Loss of IFN-γ Pathway Genes in Tumor Cells as a Mechanism of Resistance to Anti-CTLA-4 Therapy. *Cell*, (2016).
22. T. Y. Basham, T. C. Merigan, Recombinant interferon-gamma increases HLA-DR synthesis and expression. *Journal of immunology (Baltimore, Md. : 1950)* **130**, 1492-1494 (1983).
23. B. Seliger, U. Wollscheid, F. Momburg, T. Blankenstein, C. Huber, Characterization of the major histocompatibility complex class I deficiencies in B16 melanoma cells. *Cancer Res* **61**, 1095-1099 (2001).
24. W. W. Overwijk, N. P. Restifo, B16 as a mouse model for human melanoma. *Curr Protoc Immunol* **Chapter 20**, Unit 20.21 (2001).
25. R. Carretero *et al.*, Analysis of HLA class I expression in progressing and regressing metastatic melanoma lesions after immunotherapy. *Immunogenetics* **60**, 439-447 (2008).
26. T. Cabrera *et al.*, HLA class I expression in metastatic melanoma correlates with tumor development during autologous vaccination. *Cancer Immunol Immunother* **56**, 709-717 (2007).
27. E. A. Bach, M. Aguet, R. D. Schreiber, The IFN gamma receptor: a paradigm for cytokine receptor signaling. *Annual review of immunology* **15**, 563-591 (1997).
28. K. Paucker, K. Cantell, W. Henle, Quantitative studies on viral interference in suspended L cells. III. Effect of interfering viruses and interferon on the growth rate of cells. *Virology* **17**, 324-334 (1962).
29. S. J. Lee *et al.*, Interferon regulatory factor-1 is prerequisite to the constitutive expression and IFN-gamma-induced upregulation of B7-H1 (CD274). *FEBS Lett* **580**, 755-762 (2006).
30. A. Garcia-Diaz *et al.*, Interferon Receptor Signaling Pathways Regulating PD-L1 and PD-L2 Expression. *Cell Rep* **19**, 1189-1201 (2017).
31. K. E. Cole *et al.*, Interferon-inducible T cell alpha chemoattractant (I-TAC): a novel non-ELR CXC chemokine with potent activity on activated T cells through selective high affinity binding to CXCR3. *The Journal of experimental medicine* **187**, 2009-2021 (1998).
32. J. M. Farber, A macrophage mRNA selectively induced by gamma-interferon encodes a member of the platelet factor 4 family of cytokines. *Proceedings of the National Academy of Sciences of the United States of America* **87**, 5238-5242 (1990).
33. A. D. Luster, J. C. Unkeless, J. V. Ravetch, Gamma-interferon transcriptionally regulates an early-response gene containing homology to platelet proteins. *Nature* **315**, 672-676 (1985).
34. J. L. Benci *et al.*, Opposing Functions of Interferon Coordinate Adaptive and Innate Immune Responses to Cancer Immune Checkpoint Blockade. *Cell* **178**, 933-948.e914 (2019).

35. M. Donia *et al.*, Acquired Immune Resistance Follows Complete Tumor Regression without Loss of Target Antigens or IFNgamma Signaling. *Cancer Res* **77**, 4562-4566 (2017).
36. J. Girdlestone, M. Isamat, D. Gewert, C. Milstein, Transcriptional regulation of HLA-A and -B: differential binding of members of the Rel and IRF families of transcription factors. *Proceedings of the National Academy of Sciences of the United States of America* **90**, 11568-11572 (1993).
37. P. Mansky, W. M. Brown, J. H. Park, J. W. Choi, S. Y. Yang, The second kappa B element, kappa B2, of the HLA-A class I regulatory complex is an essential part of the promoter. *Journal of immunology (Baltimore, Md. : 1950)* **153**, 5082-5090 (1994).
38. M. Forloni *et al.*, NF-kappaB, and not MYCN, regulates MHC class I and endoplasmic reticulum aminopeptidases in human neuroblastoma cells. *Cancer Res* **70**, 916-924 (2010).
39. Y. Cheng, N. J. King, A. M. Kesson, Major histocompatibility complex class I (MHC-I) induction by West Nile virus: involvement of 2 signaling pathways in MHC-I up-regulation. *J Infect Dis* **189**, 658-668 (2004).
40. S. Heidegger *et al.*, RIG-I activation is critical for responsiveness to checkpoint blockade. *Sci Immunol* **4**, (2019).
41. J. J. Ishizuka *et al.*, Loss of ADAR1 in tumours overcomes resistance to immune checkpoint blockade. *Nature*, (2018).
42. F. A. Ran *et al.*, Genome engineering using the CRISPR-Cas9 system. *Nat Protoc* **8**, 2281-2308 (2013).
43. S. C. Wei *et al.*, Distinct Cellular Mechanisms Underlie Anti-CTLA-4 and Anti-PD-1 Checkpoint Blockade. *Cell* **170**, 1120-1133.e1117 (2017).
44. H. Chen *et al.*, Cytofkit: A Bioconductor Package for an Integrated Mass Cytometry Data Analysis Pipeline. *PLoS Comput Biol* **12**, e1005112 (2016).
45. D. Kim, J. M. Paggi, C. Park, C. Bennett, S. L. Salzberg, Graph-based genome alignment and genotyping with HISAT2 and HISAT-genotype. *Nature biotechnology* **37**, 907-915 (2019).
46. S. Anders, P. T. Pyl, W. Huber, HTSeq--a Python framework to work with high-throughput sequencing data. *Bioinformatics* **31**, 166-169 (2015).
47. M. I. Love, W. Huber, S. Anders, Moderated estimation of fold change and dispersion for RNA-seq data with DESeq2. *Genome Biol* **15**, 550 (2014).
48. A. A. Sergushichev, An algorithm for fast preranked gene set enrichment analysis using cumulative statistic calculation. *bioRxiv*, 060012 (2016).
49. A. Liberzon *et al.*, The Molecular Signatures Database (MSigDB) hallmark gene set collection. *Cell systems* **1**, 417-425 (2015).
50. H. Wickham, *ggplot2: Elegant Graphics for Data Analysis*. (Springer Publishing Company, Incorporated, 2009).

Acknowledgments We thank William H. McBride, PhD and Cristina Puig-Saus, PhD for scientific discussion and feedback. We acknowledge the UCLA Flow Cytometry Core and the Broad Stem Cell Research Center Flow Cytometry, and in particular Dr. Alejandro Garcia and Iris Williams for assistance with flow and mass cytometry and cell sorting; the UCLA Technology Center for Genomics and Bioinformatics for RNA sequencing support; and the UCLA Department of Radiation Oncology Mouse Core for assistance with mouse experiments. **Funding** This study was funded in part by the Parker Institute for Cancer Immunotherapy (A.R.), NIH grants R35 CA197633 (A.R.), P01 CA244118 (A.R.) and P01 CA168585 (A.R.), the Ressler Family Fund (A.R.) and the support from Ken and Donna Schultz (A.R.). The study was also supported by UCLA CTSI KL2 Award (NCATS TR001882; A.K.), Sarcoma Alliance for Research Through Collaboration Career Enhancement Program (A.K.), Tower Cancer Research Foundation Young Investigator Award (A.K.), and Radiological Society for North America Research Scholar Grant (A.K.). K.M.C. was supported by the NIH Ruth L. Kirschstein Institutional National Research Service Award #T32-CA009120. R.D.D. was supported by the UCLA Jonsson Comprehensive Cancer Center (JCCC). Flow and mass cytometry were performed in the UCLA JCCC and Center for AIDS Research Flow Cytometry Core Facility that is supported by NIH awards P30 CA016042 and 5P30 AI028697, the UCLA JCCC, the UCLA AIDS Institute, and the David Geffen School of Medicine at UCLA. **Author contributions** A.K. and A.R. conceived and designed the experiments. A.K., K.H., M.T., S.K., A.V-C., D.S., J.M.Z., J.M.F., R.D.D. and P.P.L. conducted experiments and analyzed the data. K.M.C. and A.K. analyzed RNA sequencing data. C.N. conducted blinded tumor measurements. D.T., A.C., and G.P. conducted experiments. D.E.S. analyzed data and revised the manuscript. A.K., M.Q. and A.R. wrote and revised the manuscript and supervised the study. **Competing interests** J.M.F.,

P.L-C. and M.Q. are employed full-time by Highlight Therapeutics and M.Q. holds stock. A.R. has received honoraria for consulting with Amgen, Bristol-Myers Squibb, Chugai, Genentech, Merck, Novartis, Roche and Sanofi, is or has been a member of the scientific advisory board, and holds stock in Advaxis, Arcus Biosciences, Highlight Therapeutics, Compugen, CytomX, Five Prime, FLX Bio, ImaginAb, IsoPlexis, Gilead Kite, Lutris Pharma, Merus, PACT Pharma, Rgenix and Tango Therapeutics. A.K. is a member of the scientific advisory board for T-Cure. A.K. and A.R. are inventors of a patent application covering the therapeutic use of BO-112 in combination with adoptive T cell therapy for cancer ("Methods for Treating Cancer Using Adoptive Cellular Therapy", provisional patent filing number 62/739,783). R.D.D. has consulted for Amgen, Epirium, Holoclara, Acurastem and Kirkland & Ellis.

Data and materials availability All data associated with this study are present in the paper or the Supplementary Materials. BO-112 was obtained through an MTA with Highlight Therapeutics. Gene expression data will be available at www.ncbi.nih.gov/geo/.

Figure 1

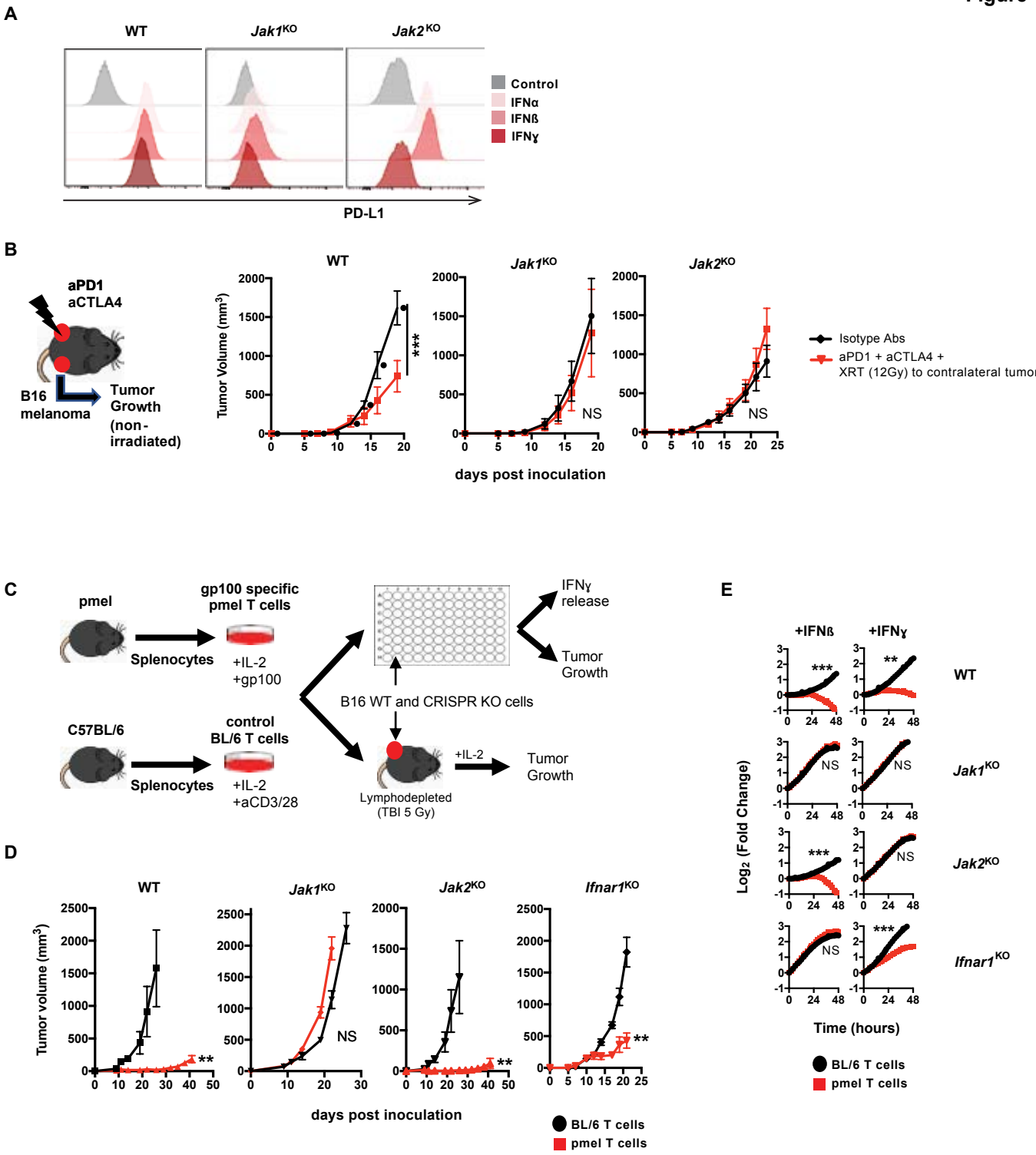
A
WT
Jak1KO
Jak2KO
Control
IFNα
IFNß
IFNɣ
PD-L1
B
aPD1
aCTLA4
B16 melanoma
Tumor Growth (non-irradiated)
WT
Jak1KO
Jak2KO
Tumor Volume (mm3)
***
NS
NS
days post inoculation
Isotype Abs
aPD1 + aCTLA4 + XRT (12Gy) to contralateral tumor
C
pmel
Splenocytes
gp100 specific pmel T cells
+IL-2
+gp100
C57BL/6
Splenocytes
control BL/6 T cells
+IL-2
+aCD3/28
B16 WT and CRISPR KO cells
IFNɣ release
Tumor Growth
+IL-2
Lymphodepleted (TBI 5 Gy)
Tumor Growth
D
WT
Jak1KO
Jak2KO
Ifnar1KO
Tumor volume (mm3)
**
NS
**
**
days post inoculation
BL/6 T cells
pmel T cells
E
+IFNß
+IFNɣ
***
**
NS
NS
***
NS
NS
***
WT
Jak1KO
Jak2KO
Ifnar1KO
Log2 (Fold Change)
Time (hours)
BL/6 T cells
pmel T cells

Figure 1. *Jak1* loss*,* but not *Jak2 or Ifnar1* loss, mediates resistance of B16 melanoma to adoptively transferred tumor-specific T cells. (A) PD-L1 surface expression by flow cytometry in response to IFNα, IFNβ, or IFNγ. (B) Tumor growth (mean +/- SEM) of non-irradiated tumors in a dual-flank model. Mice (n=4-6/group) were treated with focal tumor irradiation (12 Gy) to a contralateral tumor, along with αPD1 and αCTLA4 dual immune checkpoint blockade (or relevant isotype controls); *, $p<0.05$; **, $p<0.01$; ***, $p<0.001$ (unpaired t test) (C) In vitro and in vivo modeling of efficacy of tumor-specific pmel T cells against B16 wildtype (WT) and CRISPR-modified cell line. (D) In vivo tumor growth (mean +/- SEM) of CRISPR-modified B16-F10 tumors (WT, *Jak1*^{KO}, *Jak2*^{KO}, *Ifnar1*^{KO}) after treatment with adoptive cell therapy. After lymphodepleting total body irradiation (5Gy), tumor-bearing mice (n=5/group) were treated with adoptive cell therapy consisting of one dose of $5.0x10_6$ pmel (or control BL/6 T cells) along with IL-2 (50,000 IU/day i.p. x 3 days). **, $p<0.01$ (repeated measures 2-way ANOVA). (E) In vitro growth (mean +/- SD) of CRISPR-modified B16-F10 tumor cell lines pre-treated with either IFNβ (left panel) or IFNγ (right panel) and cocultured with tumor-specific pmel T cells (red) or control BL/6 T cells (black). Cocultures performed in biological triplicate; error bars not visible as they are encompassed within the data points. *, $p<0.05$, **, $p<0.01$; ***, $p<0.001$(unpaired t test).

Figure 2

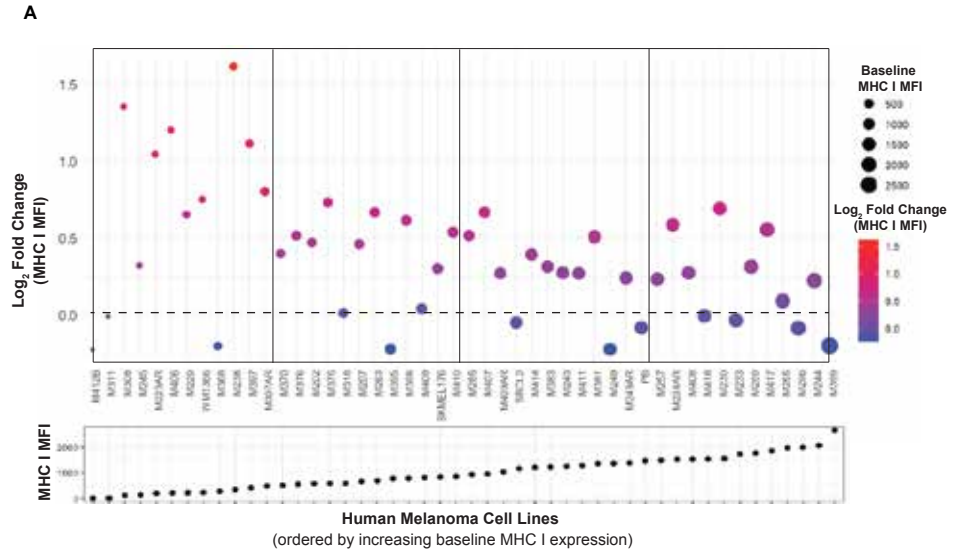
A
Log2 Fold Change (MHC I MFI)
Baseline MHC I MFI
Log2 Fold Change (MHC I MFI)
MHC I MFI
Human Melanoma Cell Lines
(ordered by increasing baseline MHC I expression)

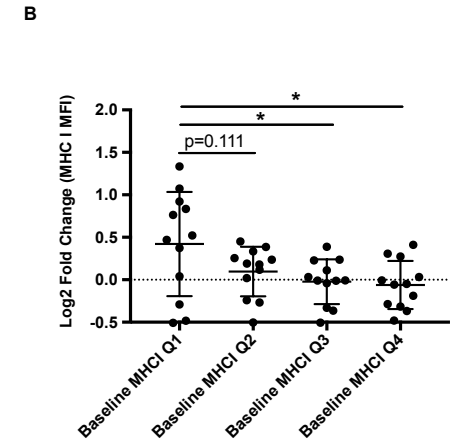
B
Log2 Fold Change (MHC I MFI)
p=0.111
Baseline MHCI Q1
Baseline MHCI Q2
Baseline MHCI Q3
Baseline MHCI Q4

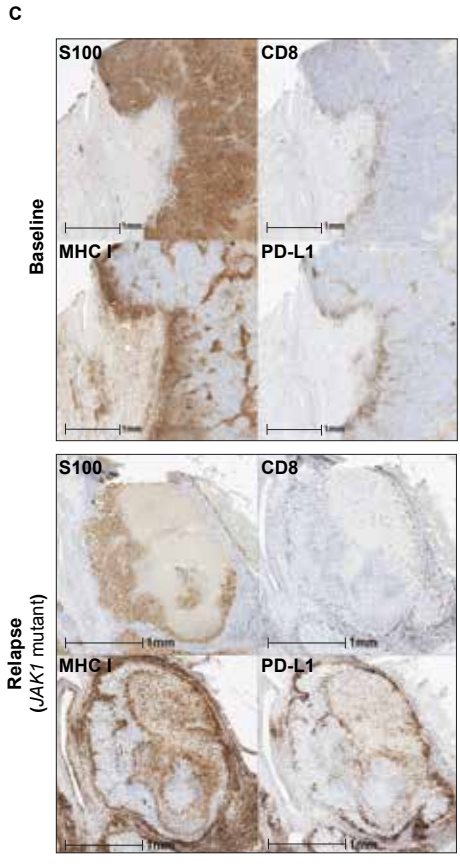
C
Baseline
S100
CD8
MHC I
PD-L1
Relapse (JAK1 mutant)

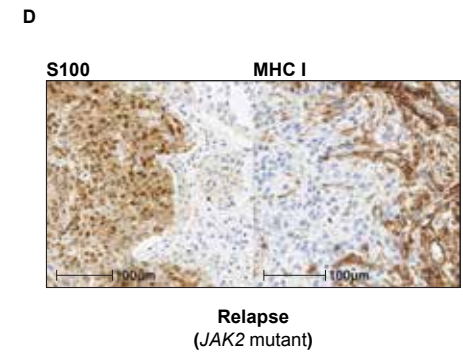
D
S100
MHC I
Relapse
(JAK2 mutant)

Figure 2 MHC I expression of human melanoma exhibits IFNγ dependence. (A) The effect of IFNγ on surface MHC I expression of 48 human melanoma cell lines. Cell lines arranged from left to right by increasing MHC I expression (basal MHC I MFI shown in bottom panel and also as the diameter of the data point in the main panel). Data is shown as log_2(fold change) of MFI of the IFNγ-treated sample relative to untreated control (and also colored from blue to red according to value of log_2(fold change). (B) Relative change in MFI (mean +/- SD) upon IFNγ exposure as related to basal MHC I expression. *, $p<0.05$ (unpaired t test). (C) Immunohistochemical staining analysis at baseline and relapse in a patient with melanoma that developed acquired genetic resistance (loss-of-function *JAK1* mutation) to anti-PD1 immune checkpoint blockade. (D) S100 (left) and MHC I (right) expression at the tumor margin in a patient with melanoma that developed acquired genetic resistance to immune checkpoint blockade vis-à-vis loss-of-function mutation in *JAK2*.

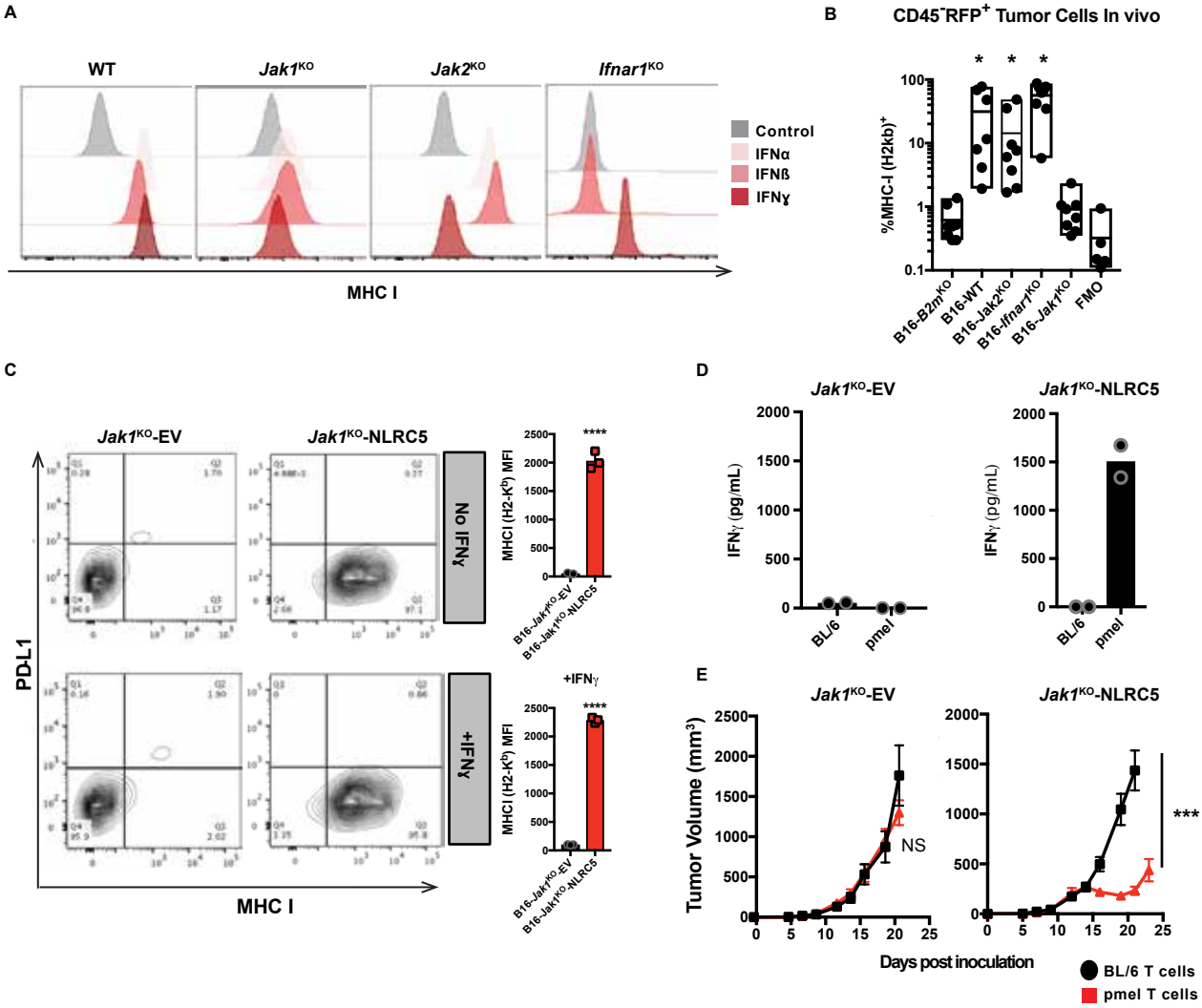
A
WT
Jak1KO
Jak2KO
Ifnar1KO
Control
IFNα
IFNß
IFNγ
MHC I
B
CD45-RFP+ Tumor Cells In vivo
%MHC-I (H2kb)+
B16-B2mKO
B16-WT
B16-Jak2KO
B16-Ifnar1KO
B16-Jak1KO
FMO
C
Jak1KO-EV
Jak1KO-NLRC5
No IFNγ
+IFNγ
PD-L1
MHC I
MHCI (H2-Kb) MFI
B16-Jak1KO-EV
B16-Jak1KO-NLRC5
D
Jak1KO-EV
Jak1KO-NLRC5
IFNγ (pg/mL)
BL/6
pmel
E
Jak1KO-EV
Jak1KO-NLRC5
Tumor Volume (mm3)
NS
Days post inoculation
BL/6 T cells
pmel T cells

Figure 3 NLRC5 bypasses IFN-dependency of B16 MHC I expression and restores sensitivity to adoptive T cell therapy. (A) MHC I surface expression by flow cytometry in response to IFNα, IFNβ, or IFNγ in CRISPR-modified B16-F10 cell lines. (B) Percentage of MHC I_+ cells among CD45-RFP_+ tumor cells in vivo. Mice (n=5-8/group) were inoculated subcutaneously with RFP_+ tumor cell lines. Established tumors were harvested and single cell suspensions were stained for CD45 and MHC I. Box plots depict minimum, maximum and mean. (C) Surface expression of PD-L1 and MHC I on B16-*Jak1*$_{KO}$ tumor cells lentivirally transduced with *Nlrc5* or empty vector control. Shown are representative samples treated with and without IFNγ and summary bar plots of MHC I MFI (mean +/- SD, n=3/group). ****, $p<0.0001$. (D) IFNγ production (mean +/- SD) by BL/6 or pmel T cells after 24-hour coculture with indicated tumor cells (which were not pre-treated with IFNγ; n=3/group). (E) In vivo tumor growth (mean +/- SEM) of B16-*Jak1*$_{KO}$-EV and B16-*Jak1*$_{KO}$-NLRC5 tumors after treatment with adoptive cell therapy. After lymphodepleting total body irradiation (5 Gy), tumor-bearing mice (n=5/group) were treated with adoptive cell therapy consisting of one dose of $5.0x10_6$ pmel (or control BL/6 T cells) along with IL-2 (50,000 IU/day i.p. x 3 days). ***, $p<0.001$ (unpaired t test).

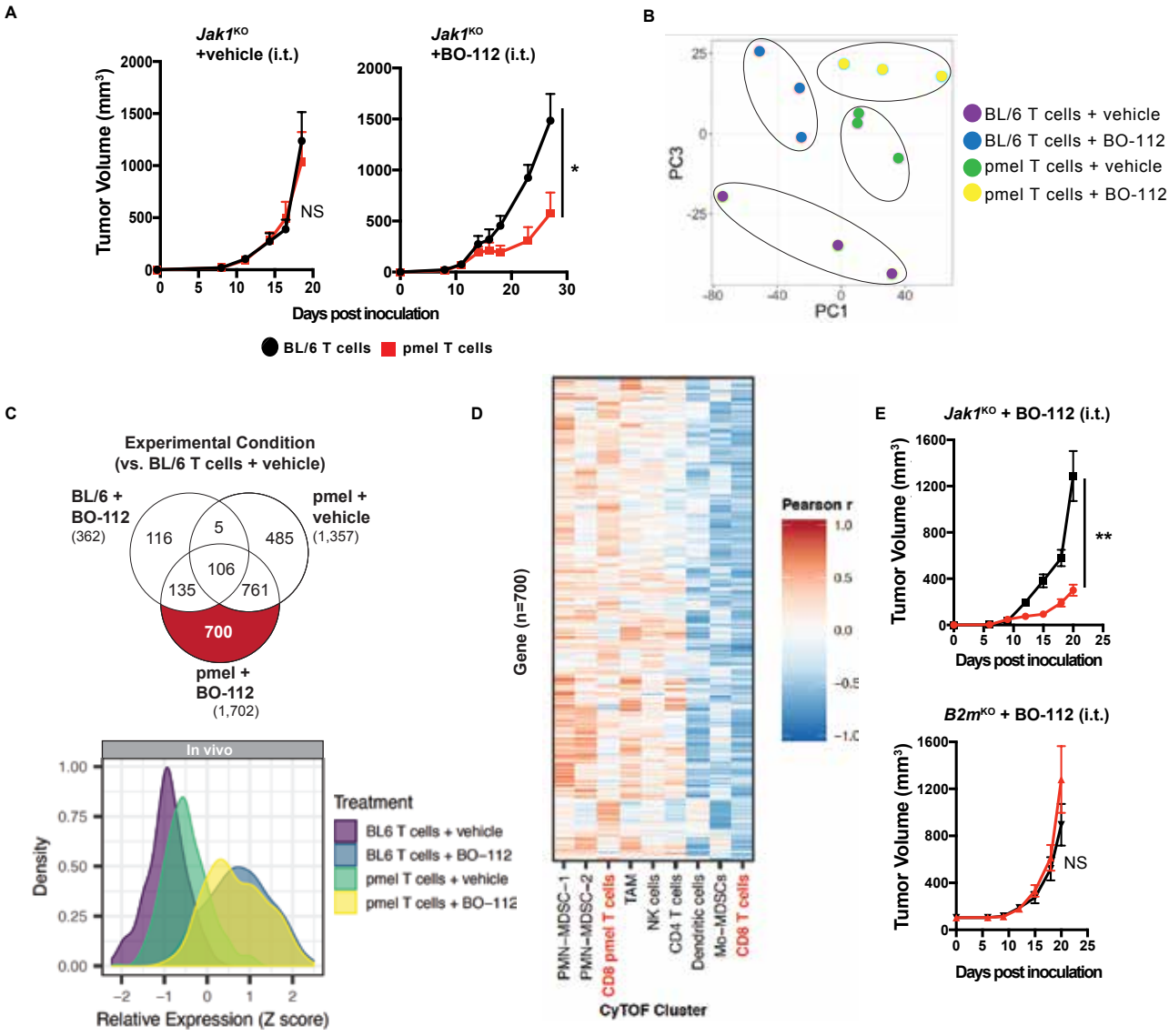
A
Jak1KO +vehicle (i.t.)
Jak1KO +BO-112 (i.t.)
Tumor Volume (mm3)
NS
*
Days post inoculation
BL/6 T cells
pmel T cells
B
PC3
PC1
BL/6 T cells + vehicle
BL/6 T cells + BO-112
pmel T cells + vehicle
pmel T cells + BO-112
C
Experimental Condition
(vs. BL/6 T cells + vehicle)
BL/6 + BO-112 (362)
pmel + vehicle (1,357)
pmel + BO-112 (1,702)
116
5
485
106
135
761
700
In vivo
Density
Relative Expression (Z score)
Treatment
BL6 T cells + vehicle
BL6 T cells + BO−112
pmel T cells + vehicle
pmel T cells + BO−112
D
Gene (n=700)
Pearson r
PMN−MDSC−1
PMN−MDSC−2
CD8 pmel T cells
TAM
NK cells
CD4 T cells
Dendritic cells
Mo−MDSCs
CD8 T cells
CyTOF Cluster
E
Jak1KO + BO-112 (i.t.)
Tumor Volume (mm3)
**
Days post inoculation
B2mKO + BO-112 (i.t.)
NS

Figure 4 BO-112 restores efficacy of tumor-specific T cells against tumor cells lacking both type I and II IFN signaling. (A) In vivo growth (mean +/- SEM) of B16-*Jak1*^{KO} tumor cells after treatment with adoptive cell therapy. After lymphodepleting total body irradiation (5 Gy), tumor-bearing mice (n=4-5 mice/group) were treated with ACT consisting of one dose of $5.0x10^6$ pmel (or control BL/6 T cells) along with IL-2 (50,000 IU/day i.p. x 3 days). In left panel, both groups were treated with intratumoral injection of vehicle control. In the right panel, both groups were treated with intratumoral injection of BO-112. Intratumoral injections were administered twice a week starting on the day after ACT. *, $p<0.05$ (unpaired t test). (B) Tumors were harvested five days after ACT (and after two doses of intratumoral vehicle or BO-112) for RNA sequencing analysis (n=3 per group). Principal component analysis demonstrates clustering of treatment groups by PC1 and PC3 (treatment groups encircled manually). (C) Top panel is a Venn Diagram illustrating the number of genes differentially expressed compared to the control group (BL/6 T cells and vehicle intratumoral agent), highlighting the 700 genes differentially expressed in the group treated with pmel ACT and intratumoral BO-112. The relative expression of this set of 700 genes is shown in the bottom panel colored by treatment group (D) Heatmap of correlations between the 700 differentially expressed genes from the pmel-BO-112 gene set with $CD45^+$ populations identified by mass cytometry. (E) In vivo growth (mean +/- SEM) of B16-*Jak1*^{KO} tumors (top panel, n=5-7 mice/group) or B16-*B2m*^{KO} tumors (bottom panel, n=7 mice/group) after treatment with adoptive cell therapy and intratumoral BO-112. ***, $p<0.001$ (unpaired t test).

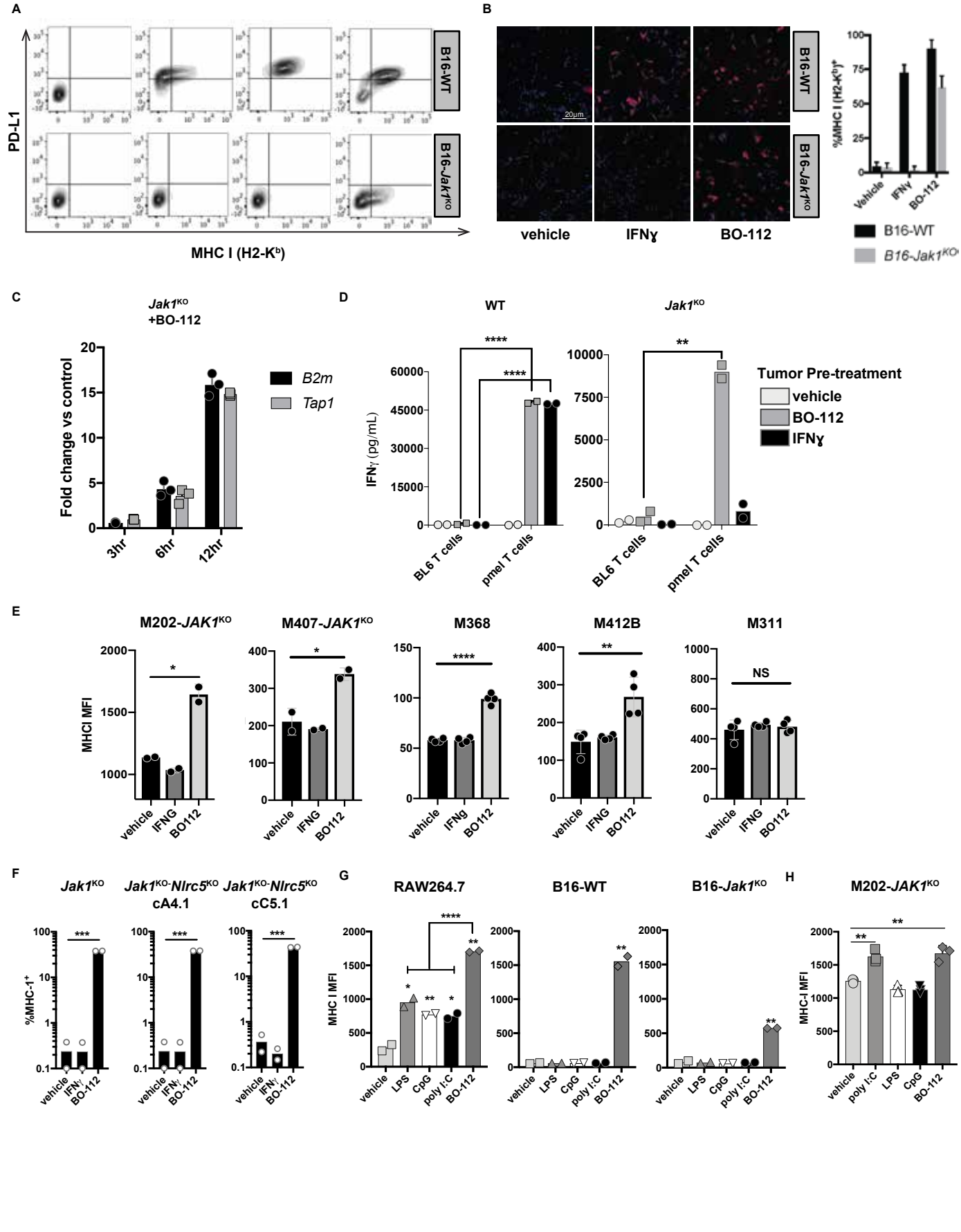
A
PD-L1
MHC I (H2-Kb)
B16-WT
B16-Jak1KO
B
20μm
vehicle
IFNɣ
BO-112
%MHC I (H2-Kb)+
Vehicle
IFNɣ
BO-112
B16-WT
B16-Jak1KO
C
Jak1KO
+BO-112
Fold change vs control
B2m
Tap1
3hr
6hr
12hr
D
WT
Jak1KO
IFNγ (pg/mL)
BL6 T cells
pmel T cells
Tumor Pre-treatment
vehicle
BO-112
IFNɣ
E
M202-JAK1KO
M407-JAK1KO
M368
M412B
M311
MHCI MFI
vehicle
IFNG
BO112
NS
F
Jak1KO
Jak1KO-Nlrc5KO
cA4.1
Jak1KO-Nlrc5KO
cC5.1
%MHC-1+
vehicle
IFNγ
BO-112
G
RAW264.7
B16-WT
B16-Jak1KO
MHC I MFI
vehicle
LPS
CpG
poly I:C
BO-112
H
M202-JAK1KO
MHC-I MFI
vehicle
poly I:C
LPS
CpG
BO-112

Figure 5 BO-112 induces MHC I expression in an interferon and *Nlrc5* independent manner. (A) Surface expression of PD-L1 and MHC I (H-2K^b) on B16-WT and B16-*Jak1*^{KO} cell lines after 18-hour exposure to IFNα, IFNβ, IFNγ, or BO-112. (B) Immunofluorescence images of B16-WT and B16-*Jak1*^{KO} cell lines treated as in (A) and stained with PE-conjugated anti-mouse MHC I (H-2K^b) and DAPI nuclear staining with quantification in the right panel (mean +/- SD; n=48 samples per treatment group). (C) Expression of genes (mean +/- SD) involved in MHC I antigen processing machinery (*B2m* and *Tap1*) by qRT-PCR in BO-112 treated B16-*Jak1*^{KO} tumor cells after 3-, 6- and 12-hours, relative to vehicle treated control (n=3/group). (D) IFNγ production (mean +/- SD) by T cells (activated BL6 T cells or pmel T cells) in coculture with B16-WT and B16-*Jak1*^{KO} tumor cells pre-treated with vehicle, BO-112 or IFNγ (n=3/group). (E) The effect of IFNγ and BO-112 on surface MHC I expression (mean +/- SD) of five human melanoma cell lines (n=2-4/group), including two with known defects in IFN signaling (M202-*JAK1*^{KO} and M407-*JAK1*^{KO}) and three cell lines with low basal MHC I expression (see Fig. 2A). (F) B16-*Jak1*^{KO} tumor cells were modified using CRISPR with guides targeting *Nlrc5* to generate two clonal B16-*Jak1*^{KO}-*Nlrc5*^{KO} cell lines (cA4.1, cC5.1). Shown is the percentage of MHC I$^+$ in each tumor cell line (mean +/- SD) after treatment with IFNγ or BO-112 for 18 hours (n=3/group). (G and H) MHC I mean fluorescence intensity (mean +/- SD) in response to a panel of pattern recognition receptor agonists (100 ng/mL LPS, 10 μg/mL CpG, 100 μg/mL poly I:C and 0.5 μg/mL BO-112) in mouse (G) and human (H) cell lines (RAW246.7 macrophages, B16-WT and B16-*Jak1*^{KO} mouse melanoma, and M202-*JAK1*^{KO} human melanoma; n=2-3/group*).* *, $p<0.05$; **, $p<0.01$; ***, $p<0.001$; ****, $p<0.0001$ (unpaired t test).

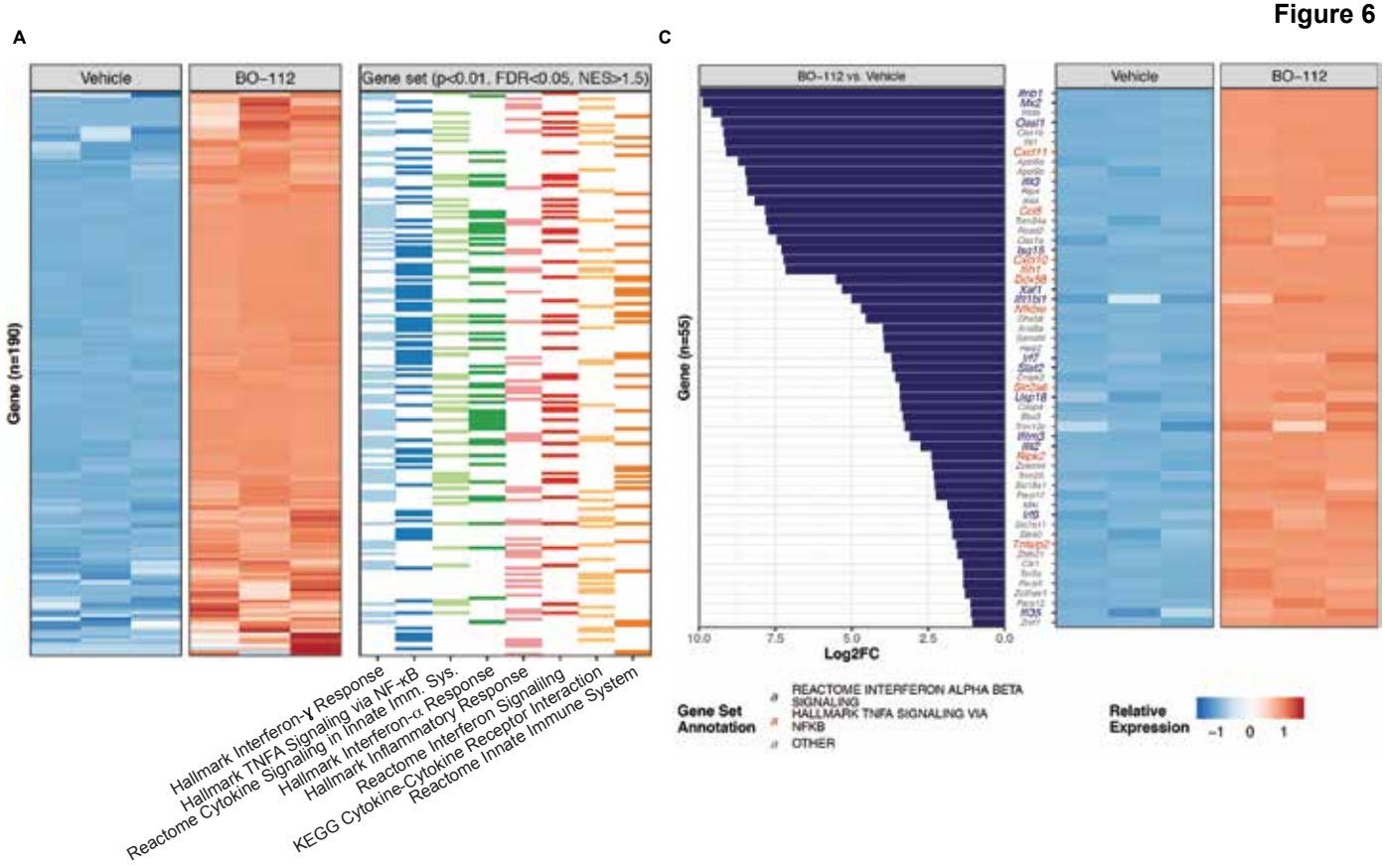
A
Vehicle
BO−112
Gene set (p<0.01, FDR<0.05, NES>1.5)
Gene (n=190)
Hallmark Interferon-γ Response
Hallmark TNFA Signaling via NF-κB
Reactome Cytokine Signaling in Innate Imm. Sys.
Hallmark Interferon-α Response
Hallmark Inflammatory Response
Reactome Interferon Signaling
KEGG Cytokine-Cytokine Receptor Interaction
Reactome Innate Immune System
C
BO−112 vs. Vehicle
Vehicle
BO−112
Gene (n=55)
Log2FC
10.0
7.5
5.0
2.5
0.0
Gene Set Annotation
REACTOME INTERFERON ALPHA BETA SIGNALING
HALLMARK TNFA SIGNALING VIA NFKB
OTHER
Relative Expression
−1
0
1

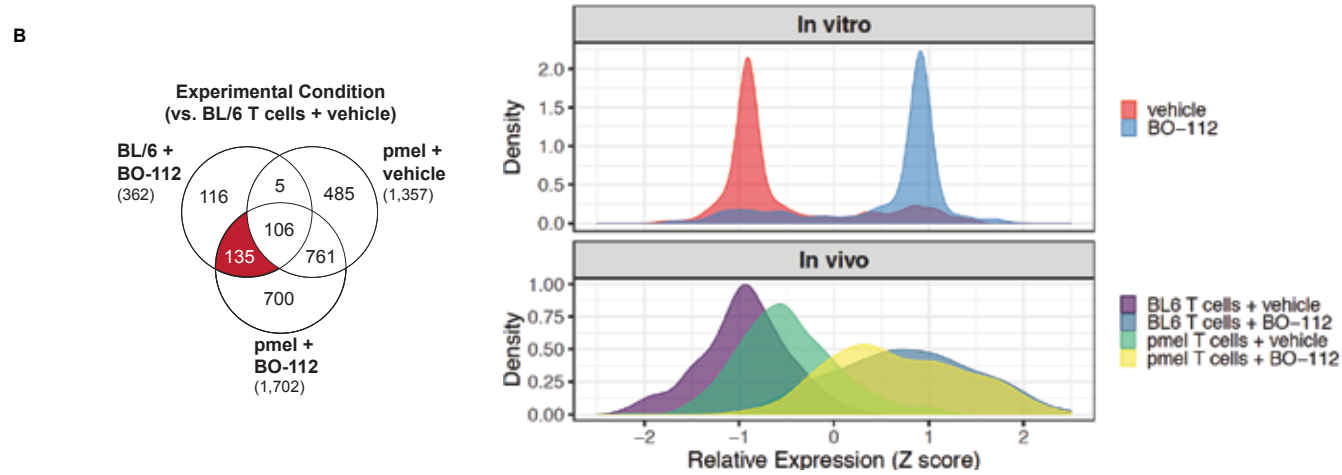
B
Experimental Condition
(vs. BL/6 T cells + vehicle)
BL/6 + BO-112 (362)
pmel + vehicle (1,357)
pmel + BO-112 (1,702)
116
5
485
106
135
761
700
In vitro
In vivo
Density
vehicle
BO−112
BL6 T cells + vehicle
BL6 T cells + BO−112
pmel T cells + vehicle
pmel T cells + BO−112
Relative Expression (Z score)

Figure 6 BO-112 induces IFN and NF-κB gene expression programs in B16-*Jak1*^{KO} tumor cells despite the absence of IFN-signaling. (A) B16-*Jak1*^{KO} tumor cell lines were treated with vehicle or BO-112 for six hours and gene expression was quantified by RNA sequencing (n=3 biological replicates). The left panel shows the top 190 differentially expressed genes ($p<0.01$, FDR<0.05, and $\log_2$(fold change)>1.5) which were also associated with significantly enriched gene sets ($p<0.01$, FDR<0.05, and normalized enrichment score>1.5). The eight enriched gene sets with at least 30 differentially expressed genes are shown in the right panel. (B) Comparison of the 136 genes enriched in tumors treated with BO-112 from our in vivo experiment (left panel; see also Fig. 4) with genes enriched in B16-*Jak1*^{KO} tumor cell line treated with BO-112. Relative expression of these 136 genes in the cell lines (right panel, top) mirrors the expression of these same genes in the groups treated with BO-112 in vivo (right panel, bottom). (C) Illustration of the in vitro $\log_2$(fold change) of 55 genes specific to BO-112 treatment both in vitro and in vivo (left panel). Enrichment of type I IFN signaling (blue) and TNF-α signaling via NF-κB (red) gene sets are highlighted. Relative expression of each gene in vitro is shown in the right panel.

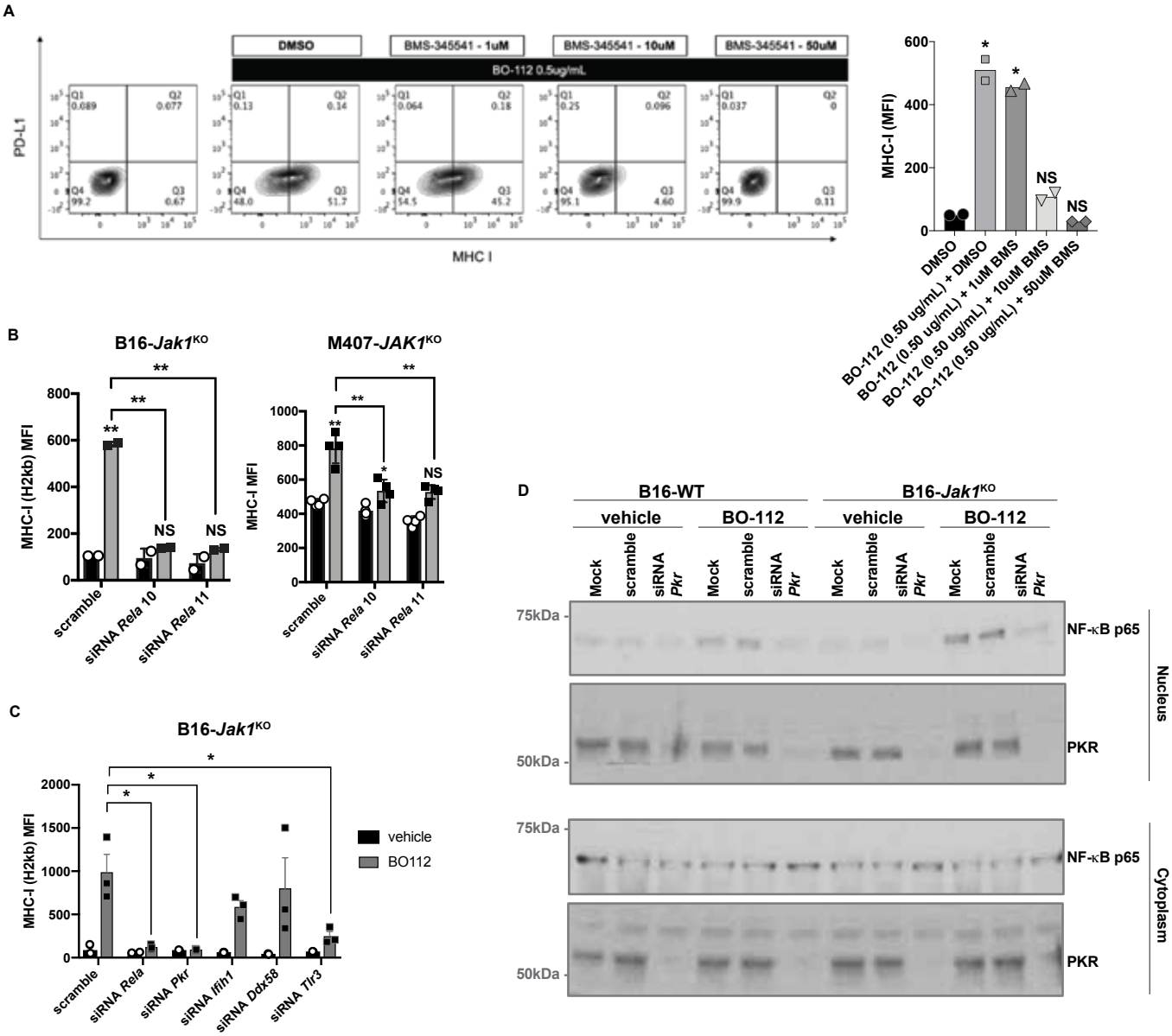
A
DMSO
BMS-345541 - 1uM
BMS-345541 - 10uM
BMS-345541 - 50uM
BO-112 0.5ug/mL
PD-L1
MHC I
MHC-I (MFI)
DMSO
BO-112 (0.50 ug/mL) + DMSO
BO-112 (0.50 ug/mL) + 1uM BMS
BO-112 (0.50 ug/mL) + 10uM BMS
BO-112 (0.50 ug/mL) + 50uM BMS
B
B16-Jak1KO
M407-JAK1KO
MHC-I (H2kb) MFI
scramble
siRNA Rela 10
siRNA Rela 11
NS
C
B16-Jak1KO
MHC-I (H2kb) MFI
vehicle
BO112
scramble
siRNA Rela
siRNA Pkr
siRNA Ifih1
siRNA Ddx58
siRNA Tlr3
D
B16-WT
B16-Jak1KO
vehicle
BO-112
Mock
scramble
siRNA Pkr
75kDa
50kDa
NF-κB p65
PKR
Nucleus
Cytoplasm

Figure 7 BO-112 bypasses IFN signaling and induces MHC class I expression through direct dsRNA sensor-mediated activation of NF-κB signaling. (A) Surface expression of MHC I and PD-L1 in in B16-*Jak1*KO tumor cells (representative example) treated with increasing doses of BMS-345541, a selective NF-κB inhibitor. Quantification shown in right panel (mean with individual data points; n=2/group). (B) Effect of siRNA targeting *Rela* on expression of MHC I in mouse B16-*Jak1*KO (mean, n=2/group) and human M407-*JAK1*KO (mean +/- SD; n=4/group) tumor cells in response to BO-112. (C) Impact of siRNAs against dsRNA sensors (*Pkr, Ifih1, Ddx588 and Tlr3)*, as well as *Rela*, on the induction of MHC I by BO-112 (mean +/- SD; n=3/group). (D) Effect of siRNA targeting *PKR* on expression of nuclear and cytoplasmic NF-kB (p65) in mouse B16-WT and B16-*Jak1*KO tumor cells in response to BO-112. *, $p<0.05$; **, $p<0.01$; ***, $p<0.001$; ****, $p<0.0001$ (unpaired t test).

Uncoupling interferon signaling and antigen presentation to overcome immunotherapy resistance in melanoma

Authors: Anusha Kalbasi*[1,3,6], Kevin Hakimi[1†], Mito Tariveranmoshabad[1†], Katie M. Campbell[2], Sarah Kremer[1], Juan M. Funes[3], Agustin Vega-Crespo[2], Giulia Parisi[2], Ameya Champekar[2], Christine Nguyen[1], Davis Torrejon[2], Daniel Shin[2], Jesse M. Zaretsky[2], Robert D. Damoiseaux[4,5,6], Daniel E. Speiser[7], Pedro P. Lopez-Casas[8], Marisol Quintero[8], Antoni Ribas[2,3,4,6,9]

SUPPLEMENTAL MATERIALS

Supplemental Figure S1: Tumor interferon signaling does not alter sensitivity of irradiated tumors to irradiation and dual immune checkpoint blockade. Tumor growth (mean +/- SEM) of irradiated tumors in a dual-flank model. Mice were treated with focal tumor-directed irradiation (12 Gy), along with αPD1 and αCTLA4 dual immune checkpoint blockade. Control mice were treated with relevant isotype controls and were not irradiated. *, p<0.05; **, p<0.01; ***, p<0.001 (unpaired t test).

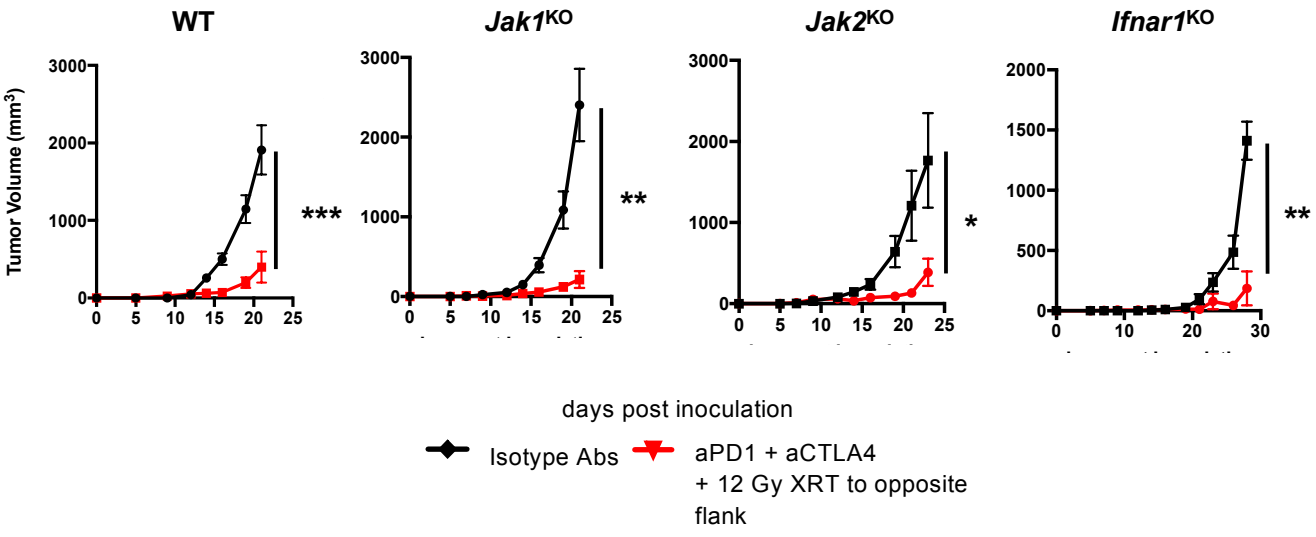

Supplementary Figure S2 CRISPR modifications of B16 tumor cell lines do not alter *gp100* expression. *gp100* gene expression (shown as ΔCT relative to *18s)* in wildtype and CRISPR-modified B16 cell lines, compared to negative control (MC38 mouse colon carcinoma cell line).

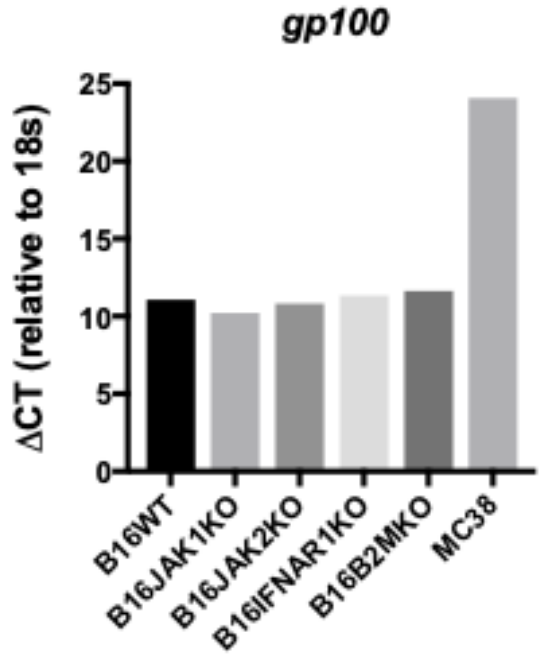

Figure S3. MHC I expression of human melanoma exhibits IFNα dependence. Cell lines arranged from left to right by increasing MHC I expression (basal MHC I MFI shown in bottom panel and also as the diameter of the data point in the main panel). Data is shown as $\log_2$(fold change) of MFI of the IFNα-treated sample relative to untreated control (and also colored from blue to red according to value of $\log_2$(fold change). Lower panel demonstrates relative change in MFI upon IFNα exposure as related to basal MHC I expression. *, p<0.05; **, p<0.01; ***, p<0.001 (unpaired t test).

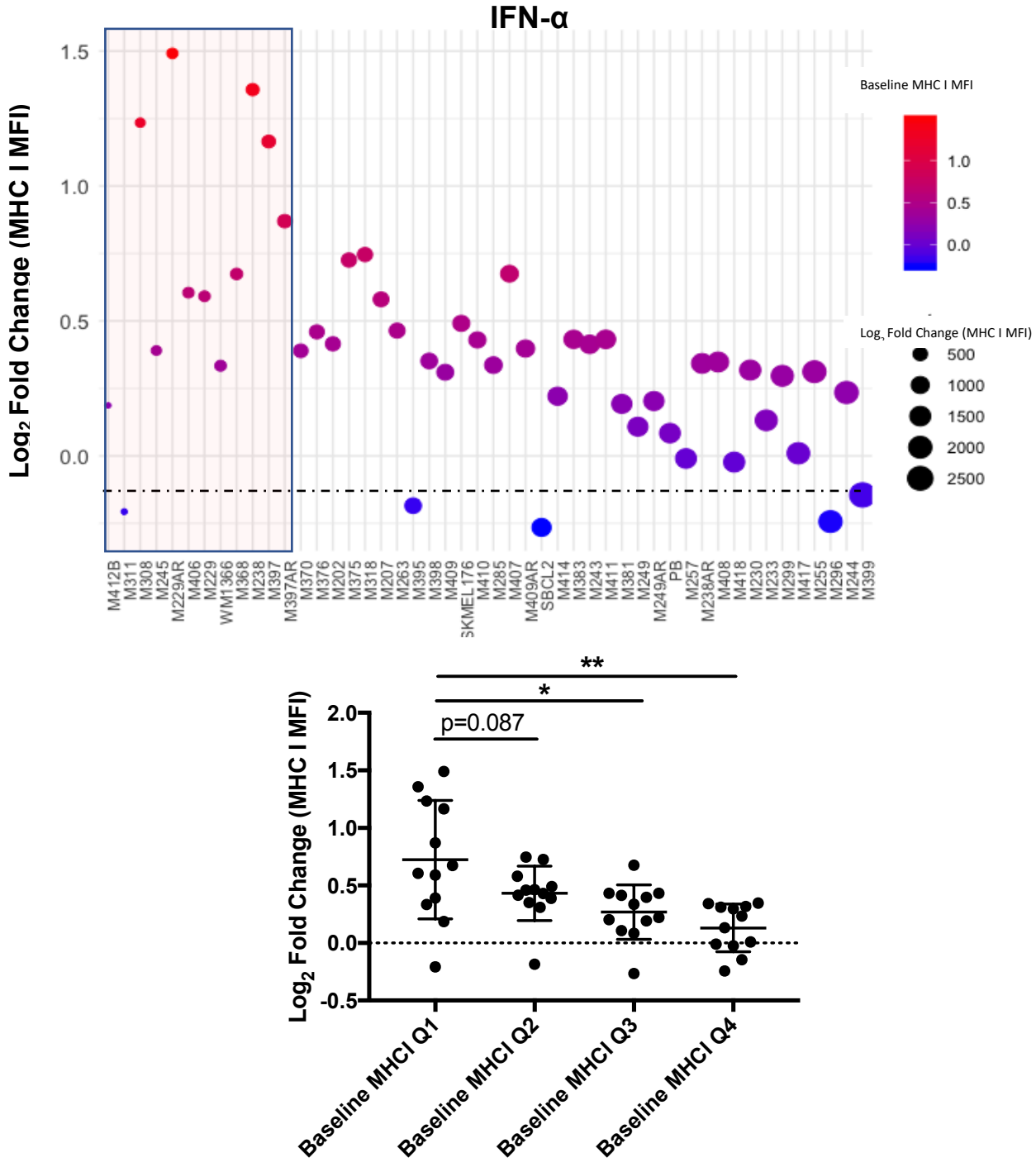

Figure S4. MHC I expression of human melanoma exhibits IFNβ-dependence. Cell lines arranged from left to right by increasing MHC I expression (basal MHC I MFI shown in bottom panel and also as the diameter of the data point in the main panel). Data is shown as $\log_2$(fold change) of MFI of the IFNβ -treated sample relative to untreated control (and also colored from blue to red according to value of $\log_2$(fold change). Lower panel demonstrates relative change in MFI upon IFNβ exposure as related to basal MHC I expression. *, p<0.05; **, p<0.01; ***, p<0.001 (unpaired t test).

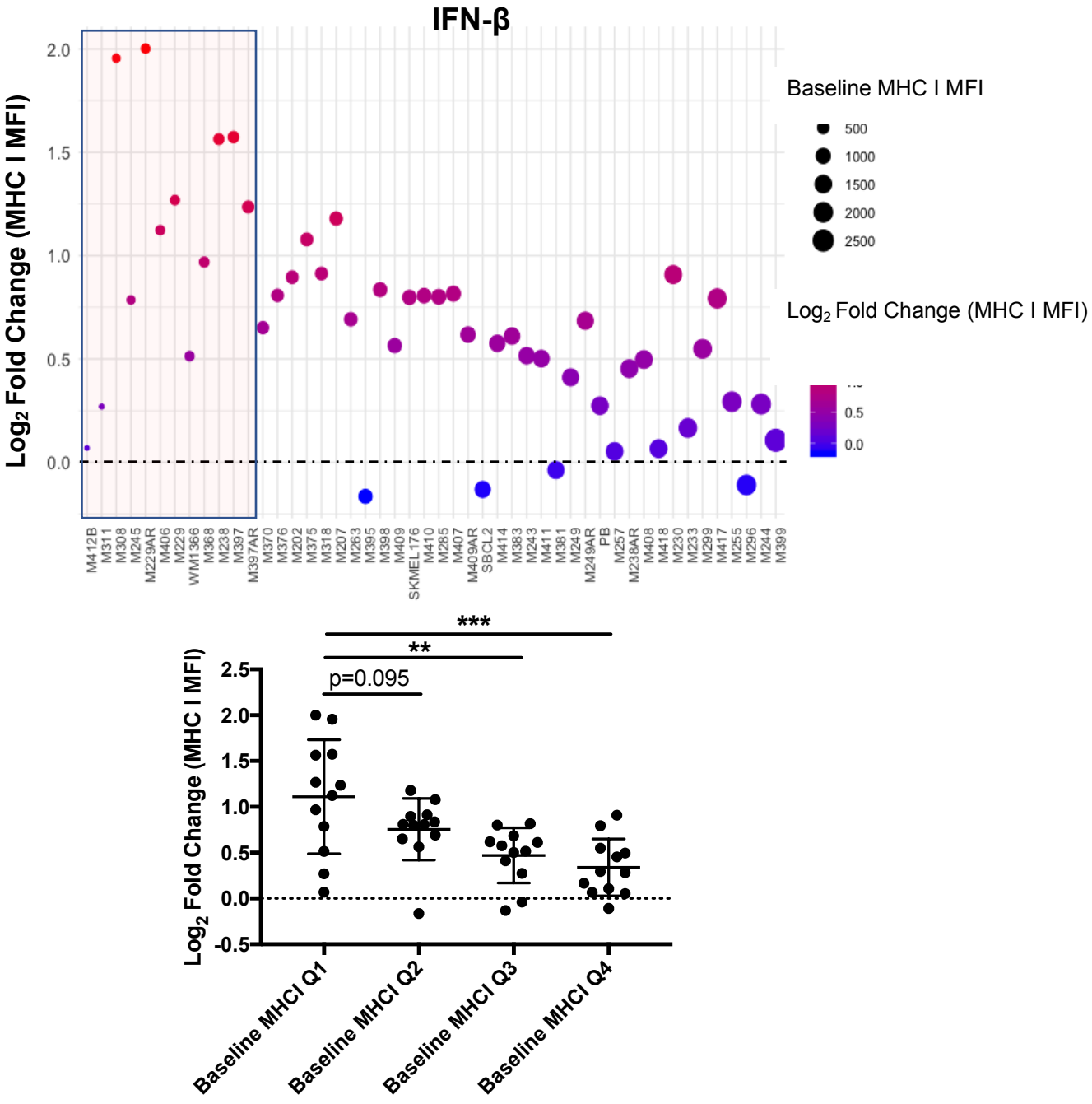

Figure S5. Gating strategy to assess in vivo MHC I expression of B16-F10. Tumor cells were gated using size and granularity (FSC/SSC), singlets (SSC-A/SSC-H), live cells (viability stain), and CD45-RFP+ cells. MHC I gate was defined using isotype control.

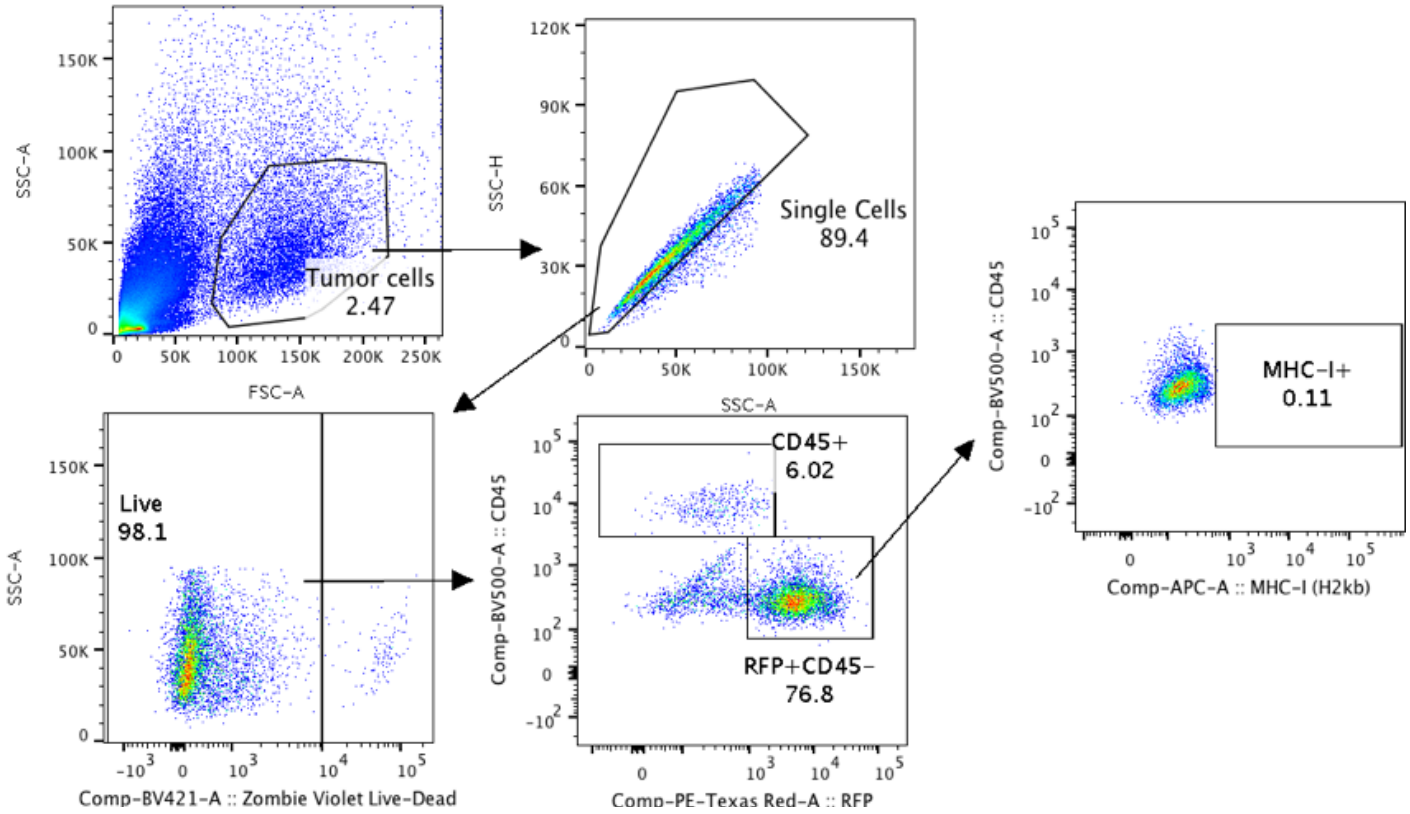

Figure S6. *Nlrc5* overexpression does not augment the anti-tumor efficacy of adoptively transferred pmel T cells against B16-WT tumors. After lymphodepleting total body irradiation (5 Gy), tumor-bearing mice were treated with adoptive cell therapy consisting of one dose of $5.0x10_6$ pmel (or control BL/6 T cells) along with IL-2 (50,000 IU/day i.p. x 3 days). ***, $p<0.001$ (unpaired t test).

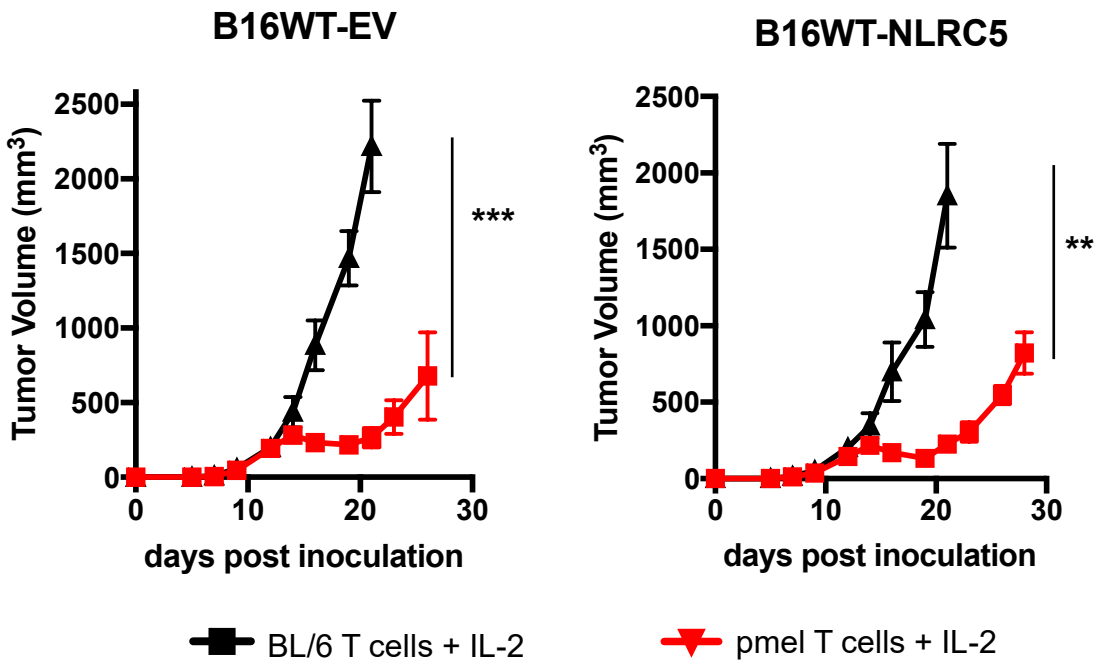

Figure S7. BO-112 augments the efficacy of pmel T cells against B16-WT tumors in vivo. In vivo growth (mean +/- SEM, n=4-5 mice/group) of B16-WT tumor cells after treatment with adoptive cell therapy (pmel versus control BL/6 T cells) and intratumoral BO-112 (or vehicle control). After lymphodepleting total body irradiation (5 Gy), tumor-bearing mice were treated with adoptive cell therapy consisting of one dose of $5.0x10_6$ pmel (or control BL/6 T cells) along with IL-2 (50,000 IU/day i.p. x 3 days). Mice received three doses of intratumoral BO-112 (or vehicle control) over seven days, starting one day after adoptive cell therapy. ***, p<0.001 (unpaired t test).

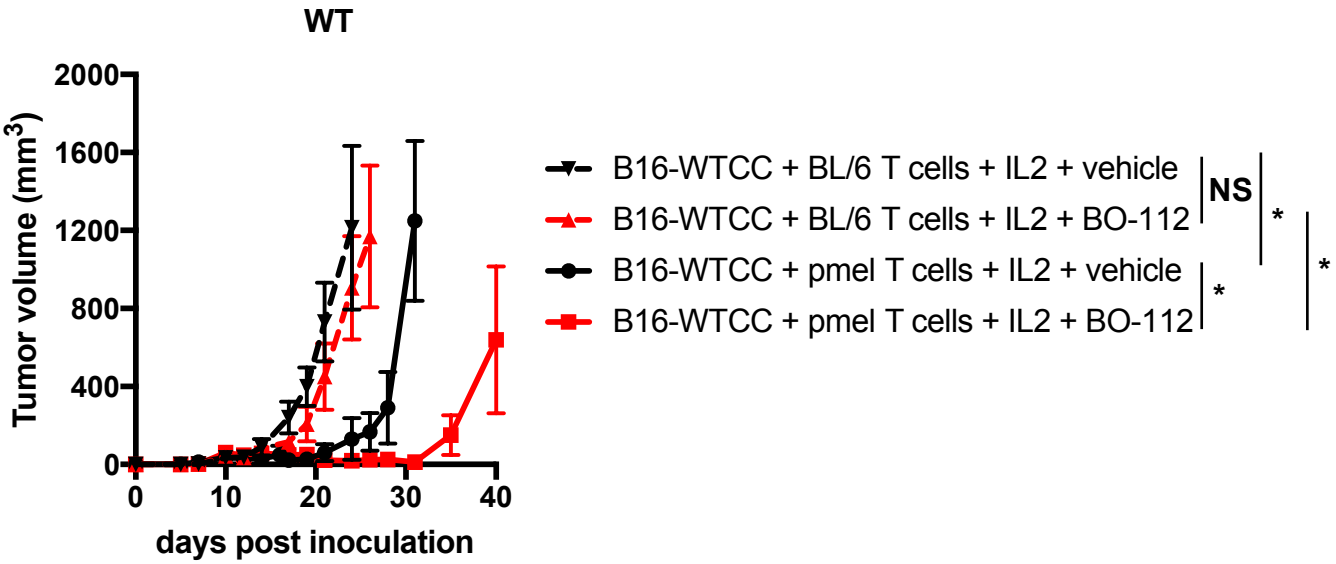

Figure S8. **BO-112 and pmel ACT alter the immune composition of B16-*Jak1*ko tumors**. Mass cytometry was performed on tumor samples (n=3) from each treatment group in parallel with RNA sequencing data described in Fig. 4B and Fig. 4C. Shown are tsne plots of mass cytometry data, restricted to CD45+ live singlets and faceted by treatment group.

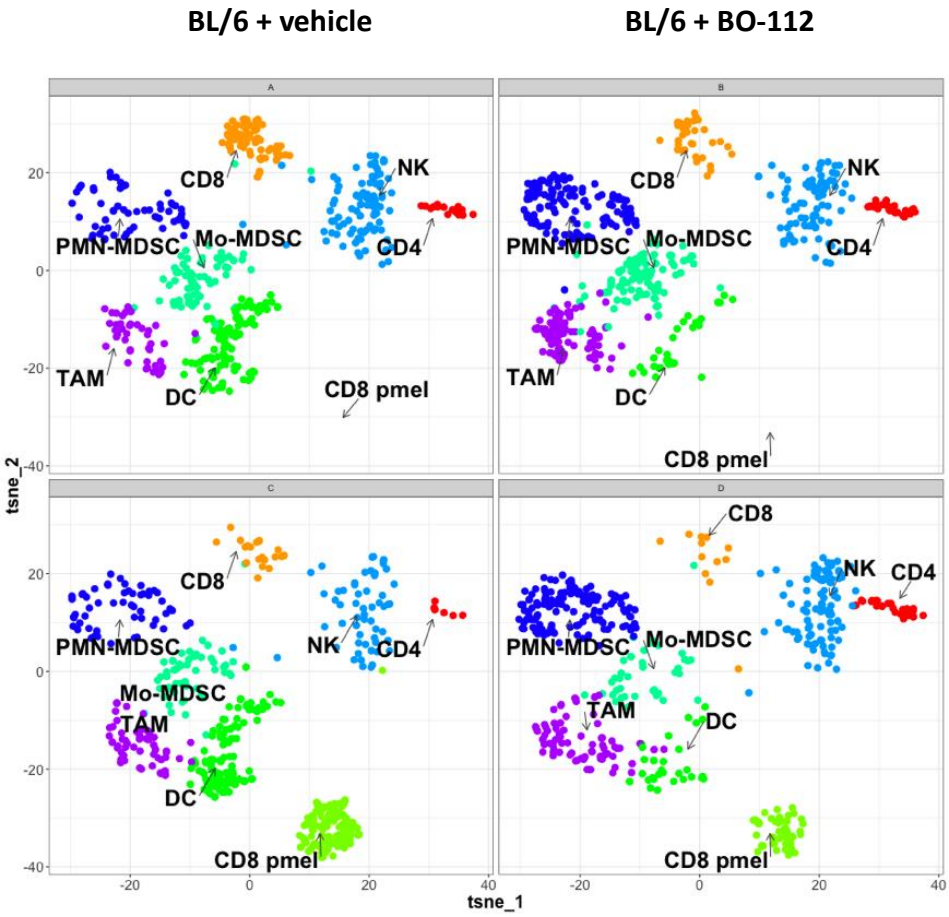

Figure S9. B16-*B2m*^{KO} tumor cells are resistant to killing by pmel T cells. In vitro tumor growth (mean +/- SD; n=3 samples per group) of B16-*B2m*^{KO} tumor cell lines pre-treated with IFNγ and cocultured with tumor-specific pmel T cells (red) or control BL/6 T cells (black).

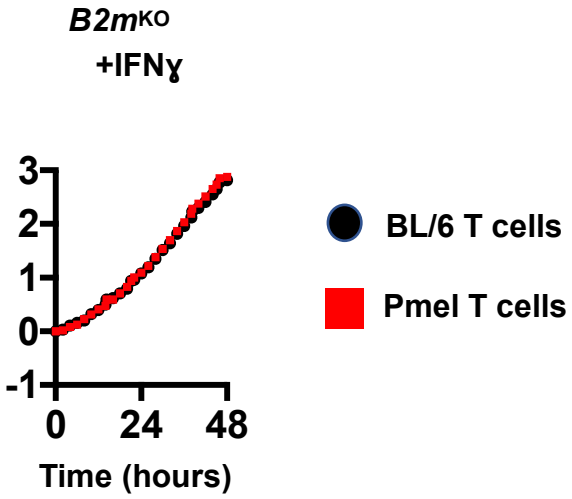

Figure S10. BO-112 induced MHC I upregulation in B16-*Jak1*^{KO} cell lines is *Nlrc5* independent. (A) Fold change (mean and individual data points) of *Nlrc5* expression by qRT-PCR upon treatment with IFNγ or BO-112 (relative to vehicle treated cells and normalized to *18s* housekeeping gene) in B16-WT and B16-*Jak1*^{KO} cell lines. (B) Flow cytometry plots corresponding to Figure 5F. B16-*Jak1*^{KO} tumor cells were modified using CRISPR with guides targeting *Nlrc5* to generate two clonal B16-*Jak1*^{KO}-*Nlrc5*^{KO} cell lines (cA4.1, cC5.1). Shown are plots of MHC I and PD-L1 expression of each tumor cell line after treatment with IFNγ or BO-112 for 18 hours. BO-112 induces MHC I in an *Nlrc5* independent manner.

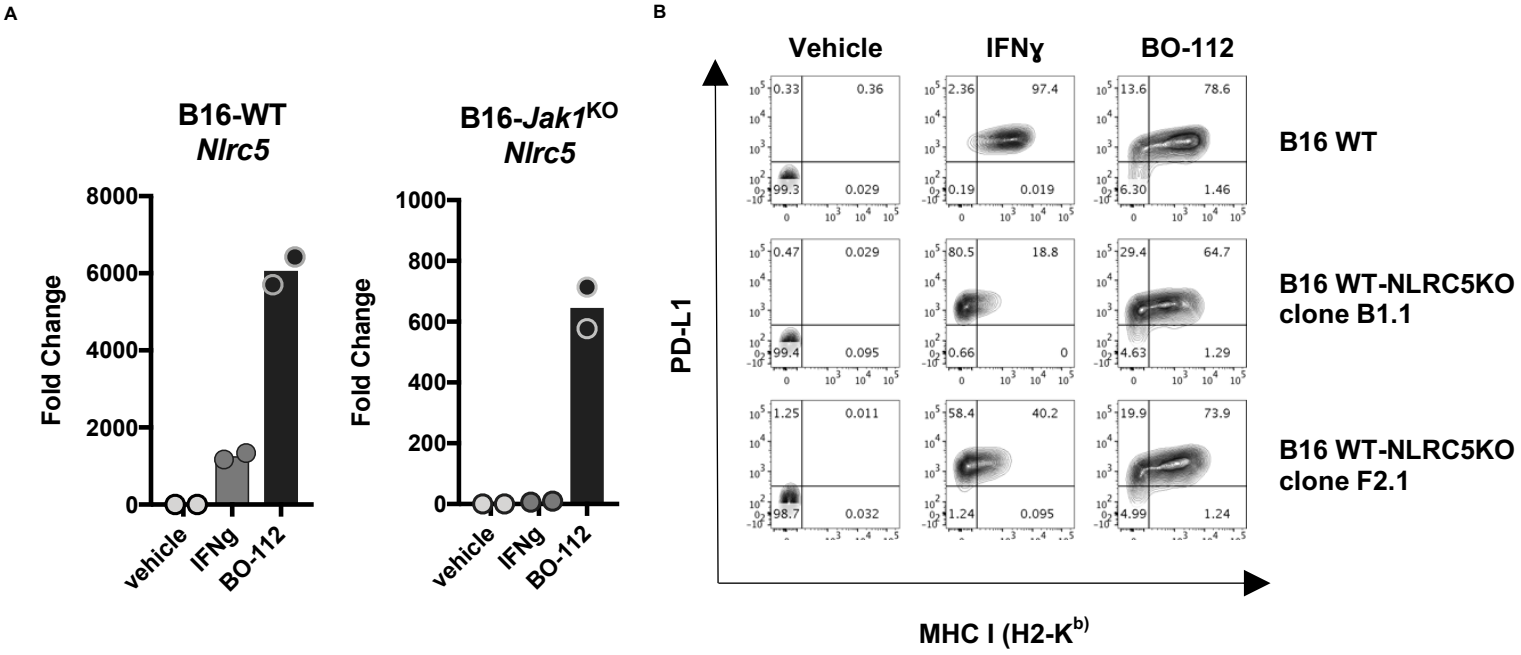

Figure S11. BO-112 induces cytoplasmic phosphorylation and nuclear translocation of NF-κB (p65) in B16-*Jak1*^{KO} cells. Western blot analysis of NF-κB (p65) (left panel) and phosphorylated NF-κB (p65) (right panel) in the cytoplasm and nucleus of B16-*Jak1*^{KO} cells after treatment with vehicle or BO-112 (0.5 μg /mL) for 5 hours.

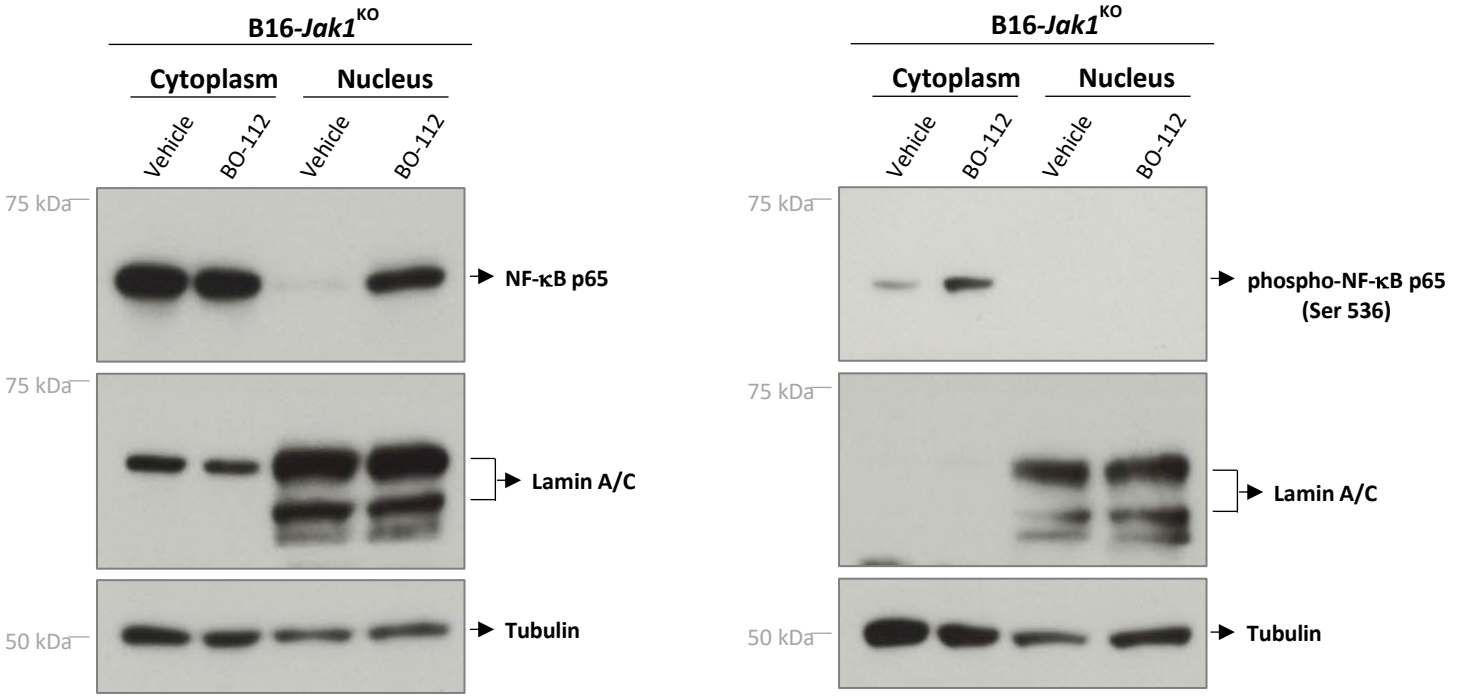

Figure S12. Protein level effects of siRNA targeting *Ifih1*, *Ddx58* or *Tlr3*. Western blot analysis of MDA-5 (A) and RIG-I (B) protein expression in B16-*Jak1*^{KO} cells after treatment with vehicle or BO-112 (0.5 μg /mL) for 18 hours, in cells treated with non-targeting control (scramble) siRNA or siRNA targeting *Ifih1* (MDA-5) or *Ddx58* (RIG-I). Western blot analysis of cytoplasmic and nuclear levels of NF-κB (p65) and PKR (C) in B16-*Jak1*^{KO} cells after treatment with vehicle or BO-112 (1.0 μg /mL) for 18 hours, after pre-treatment with non-targeting control siRNA (scramble) or siRNA targeting *Pkr* or *Tlr3*.

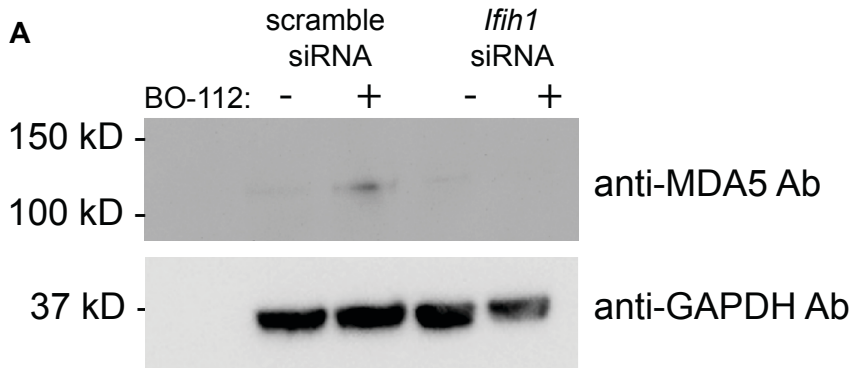

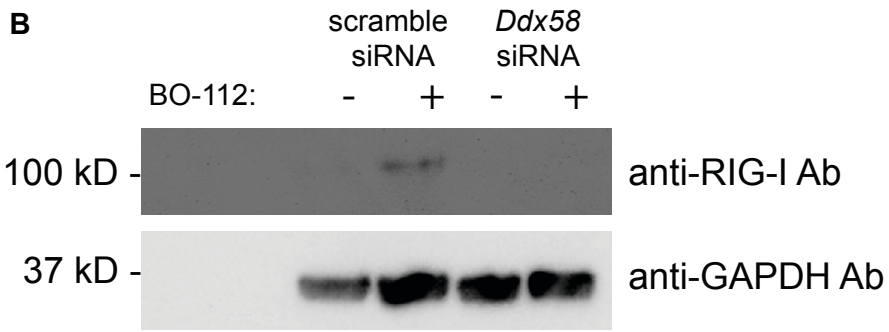

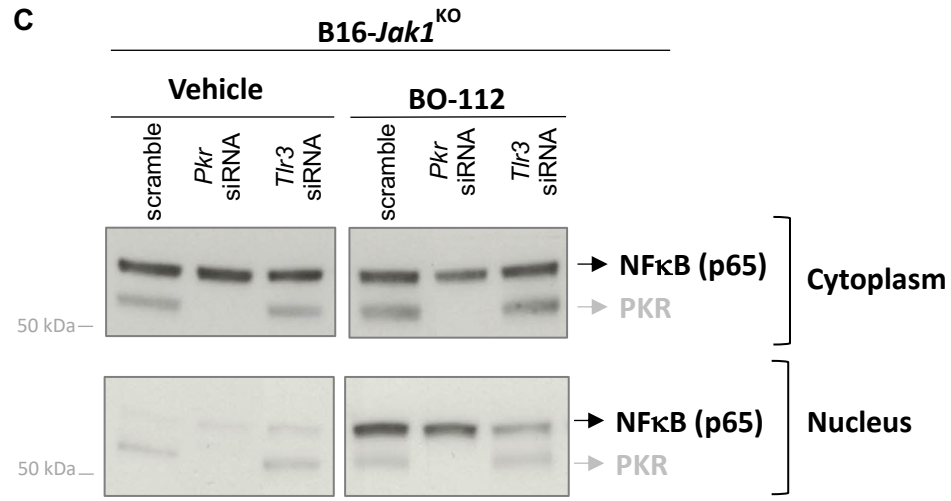

Supplementary Table 1 – CRISPR guides and RT-PCR primer sequences

Reagent	**Sequence(s)**
Murine *Jak1* CRISPR guide	CAGCGGAGAGTATACAGCCG
Murine *Jak2* CRISPR guide	CATCAGAATGGTGATATTCC
Murine *Ifnar1* CRISPR guide	GCTCGCTGTCGTGGGCGCGG
Murine *B2m* CRISPR guide	TCACGCCACCCACCGGAGAA
Murine *Nlrc5* CRISPR guide	TGGCATATCGGCTCCGCTGG
Murine *gp100* RT-PCR primers	FWD: CCTCCTTTTCCATTGCCCTG REV: AGGGAAGACACAGGCATCAT
Murine *B2m* RT-PCR primers	FWD: CGGCCTGTATGCTATCCAGA REV: ATTTCAATGTGAGGCGGGTG
Murine *Tap1* RT-PCR primers	FWD: CGCTGGAGTTTGCAAGTGAT REV: TGTCCTCAGTCACCCGAGAT
Murine *Nlrc5* RT-PCR primers	FWD: CGCCTCTCCTTCCACAATTT REV: GTCTTCAGGCTCCCCATAGT
Murine *18s* RT-PCR primers	FWD: GTAACCCGTTGAACCCCATT REV: CCATCCAATCGGTAGTAGCG

Supplementary Table 2 – Reagents

Reagent Type	Reagent	Company	Catalog #
siRNA	scramble	Ambion	AM4611
siRNA	mouse *Rela*	Ambion	AM16708
siRNA	mouse *Pkr*	Dharmacon	J-040807-05-0010
siRNA	Mouse *Rig-I*	Santa Cruz Biotechnology	sc-61481
siRNA	Mouse *Tlr3*	Santa Cruz Biotechnology	sc-40259
siRNA	Human *RELA*	Ambion	AM16708
Antibody	Anti-mouse CD45 (89Y), clone 30-F11	Biolegend	103120
Antibody	Anti-mouse CD11c (142^{Nd}), clone N418	Biolegend	117302
Antibody	Anti-mouse CD69 (143Nd), clone H1.2F23	Biolegend	104502
Antibody	Anti-mouse F4/80 (146Nd), clone BM8	DVS	31460008B
Antibody	Anti-mouse CD11b (148Nd), clone M1/70	Biolegend	101214
Antibody	Anti-mouse CD19 (149Nd), clone 6D5	Biolegend	115514
Antibody	Anti-mouse Ly6C (150Nd), clone HK1.4	Biolegend	128002
Antibody	Anti-mouse Ly6G (151Eu), clone 1A8	Biolegend	127602
Antibody	Anti-mouse CD3e (152Sm), clone 145-2C11	Biolegend	100314
Antibody	Anti-mouse CD274 (153Eu), clone 10F.9G2	DVS	3153016B
Antibody	Anti-mouse CD25 (155Gd), clone 3C7	Biolegend	101906
Antibody	Anti-mouse CD279 (159Tb), clone 29F.1A12	Biolegend	135202
Antibody	Anti-mouse CD335 (167Er), clone 29A1.4	DVS	137614
Antibody	Anti-mouse CD8 (168Er), clone 53-6.7	Biolegend	100716
Antibody	Anti-mouse CD161 (170Er), clone D13.14.4E	Biolegend	108712
Antibody	Anti-mouse CD44 (171Yb), clone IM7	Biolegend	103014
Antibody	Anti-mouse CD4 (172Yb), clone RM4-5	Biolegend	100561
Antibody	Anti-mouse MHC II (IA/IE) (174Yb), clone M5/114.15	Biolegend	107610
Antibody	Anti-mouse CD103 (175Lu), clone 2E7	Biolegend	121402
Antibody	Anti-mouse CD45R/B220 (176Yb), clone RA3-6B2	DVS	3176002B
Antibody	Anti-mouse Ki67 (115In), clone SolA15	eBioscience	14-5698-82
Antibody	Anti-mouse IFNγ (165Ho), clone XMG1.2	Invitrogen	16-7311-85
Antibody	Anti-mouse TNFα (141Pr), clone MP6-XT22	DVS	3141013B
Antibody	Anti-mouse FoxP3 (158Gd), clone FJK-16s	Invitrogen	14-5773-82
Antibody	Anti-mouse CD45 (BV510), clone 30F11	BD Biosciences	563891
Antibody	Anti-mouse H-$2K^b$ (APC), clone AF6-88.5	Biolegend	116518
Antibody	Anti-mouse PD-L1 (PE), clone MIH7	Biolegend	155404
Antibody	Anti-human HLA-A,B,C (PE-Cy7), clone W6/32	Biolegend	311430
Antibody	Anti-human PD-L1 (APC), clone MIH3	Biolegend	374514
Antibody	Anti-mouse NF-κB p65, clone L8F6	Cell Signaling Technologies	6956S
Antibody	Anti-mouse PKR, clone B-10	Santa Cruz Biotechnology	sc-6282
Antibody	Anti-mouse Phospho-NF-κB p65 (Ser536), clone 93H1	Cell Signaling Technologies	3033S
Antibody	Anti-mouse Lamin A/C, polyclonal	Cell Signaling Technologies	2032
Antibody	Anti-mouse alpha-Tubulin (clone B-5-1-2)	Sigma	T6074
Antibody	Anti-mouse RIG-I (clone D14G6)	Cell Signaling Technologies	3743S
Antibody	Anti-mouse MDA-5 (clone D74E4)	Cell Signaling Technologies	5321
Antibody	Anti-mouse GAPDH (clone 14C10)	Cell Signaling Technologies	2118